Study of a Molecular Promoter for Enhancing Cisplatin Cancer Chemotherapy

by

Jenny Nguyen

A thesis
presented to the University of Waterloo
in fulfillment of the
thesis requirement for the degree of
Master of Science
in
Physics

Waterloo, Ontario, Canada, 2010

Author's Declaration

I hereby declare that I am the sole author of this thesis. This is a true copy of the thesis, including any required final revisions, as accepted by my examiners.

I understand that my thesis may be made electronically available to the public.

Abstract

Cisplatin is one of the most widely used chemotherapeutic anti-cancer drugs due to its ability to effectively damage DNA and cause cell death. Despite this, cisplatin still suffers from two main drawbacks: toxicity and drug resistance. Many cisplatin-like compounds have been synthesized via traditional methods of drug design but very few have been able to enter clinical trials or even be approved for clinical use. The reason why so many compounds have been rejected is that their reaction mechanisms are rarely understood. By observing and studying the reaction mechanisms of a drug at the molecular level, the reaction can be optimized to enhance its therapeutic effects. The powerful technique of time-resolved pump-probe femtosecond laser spectroscopy was performed by Lu et al. to reveal the extremely high reactivity of cisplatin with weakly-bound electrons, thus providing a deeper understanding of this drug's therapeutic effects. Taking advantage of this reaction mechanism, a molecular promoter can be identified to amplify the therapeutic efficacy of cisplatin by combination in a synergistic manner. Through cell survival rate measurements, fluorescence microscopic studies to view cell death, cell cycle analysis and DNA fragmentation measurements via flow cytometry, as well as absorption spectroscopic studies, the synergistic effects between cisplatin and a new molecular promoter (PM2A) were measured. This new chemotherapeutic regimen, which was designed based on the electron-transfer reaction mechanism of cisplatin, can be used to decrease the required doses of cisplatin used in the clinic (to effectively reduce its toxic side effects), to circumvent the drug resistance and to improve targeting to cancer cells.

Acknowledgements

I would like to first thank my mentor, Dr. Qing-Bin Lu for his patience, guidance and support. I deeply appreciate his hope and desire for his students to be highly successful in their future endeavors.

I would also like to thank my committee members Dr. Jeff Chen and Dr. Kesen Ma for their thoughts and suggestions, as well as Dr. Bae-Yeun Ha for agreeing to be my external committee member. Your precious advice and time are greatly appreciated.

The administrative staff in the physics department have been extremely helpful; in particular, many thanks to Judy McDonnell for taking care of the little but very important details. Also, I am very grateful to Mishi Savulescu for her technical skills in the flow cytometry experiments.

I am very lucky to have had the opportunity to work with some amazing people in the Femtomedicine lab, who have become my second family. I would like to thank the past and present members of the lab, including: Dr. Philip Chan, Dr. Hu Xu, Dr. Jianqing Yu, Dr. Ellie Gallo-Hendrix, Dr. Dongping Qi, Dr. Huiying Ding, Chunrong Wang, Ting Luo, Yuhan Ma, Emily Miller-Cushon, Thomas Kim and Roger Liu. Support and interactions with you in between experiments made me realize what I want to be when I grow up.

I am also extremely lucky and thankful to have made some true friends during my undergraduate career. Thank you to Robbie, Ewan, Bert and Brad for all the words of encouragement throughout my studies.

Most importantly, I would like to acknowledge my best friends. Thank you Mom and Dad for all your sacrifices. Thank you also for making my life fulfilling by giving me siblings. Thanks to Karen, Vivian, Antony and also Mitsy for always telling me what I need to hear. My grandparents, uncles, aunts and cousins also deserve special mention. Your hopes and dreams keep me grounded whenever I lose sight of what I’m trying to achieve.

I would also like to acknowledge the financial support for this work: Ontario Graduate Scholarship (OGS), Canadian Institutes of Health Research (CIHR) and Natural Sciences and Engineering Research Council of Canada (NSERC).

Dedication

To my family.
All the calluses I've developed,
leading up to this point and beyond,
are all for you.

Table of Contents

List of Figures

Chapter 1. Introduction

Although the use of chemotherapeutic drugs to treat cancers is so vast, patients still suffer from extremely poor prognosis. Chemotherapy is especially used for advanced cancer patients and is also often combined with radiotherapy or surgery. Ironically, many patients die from the toxicities of the drug(s) even before the cancers completely take over their bodies. To try to increase their efficacies, chemotherapeutic drugs are often combined in regimens that allow the drugs to be administered at lower doses, but at the expense of spreading the toxicities to several sites of the body [1,2,3]. Even though many research groups have tried to form combinational chemotherapeutic regimens to combat extreme drug toxicities, they have been unsuccessful in reaching clinical uses. These disappointing results have led us to believe that a new approach to designing combinational regimens is severely needed.

Section 1.1: General Cancer Treatment

The three main modalities of cancer treatment are surgery, radiation therapy and chemotherapy. The type of treatment a patient receives depends on the location and type of the cancer, as well as the physical and emotional well-being of the patient. Surgery is used to physically remove as much of the tumor mass as possible. Radiation therapy is the use of ionizing radiation to kill cancer cells by damaging their DNA, thus disabling the cells from growing and further dividing. Cancer chemotherapy is the use of drugs to

kill the cancer cells. In general, surgery and radiotherapy provide localized treatments to the tumor, whereas chemotherapy is less specific and is non-localized. It is also quite common for a patient to receive a combination of these treatment modalities. For example, a patient may receive radiation before or after their surgery either to shrink the tumor or to get rid of residual cancer cells, respectively [4].

New treatment methods have emerged over the years, including immunotherapy, photodynamic therapy and gene therapy. Although these methods are rarely used, immense efforts are being put forth to make these methods more clinically relevant and effective [4].

Section 1.2: Chemotherapy

The first anti-cancer agent introduced into clinical trial was the nitrogen mustard (methyl-bis[chloroethyl]amine hydrochloride), which was derived from the sulfur mustard that was used during World War I as an offensive weapon. It was found that at low concentrations, the mustard gas could incapacitate the enemies by causing irritation to the respiratory tract and the eyes. It was then realized that the mustard gas had strong effects on rapidly dividing cells such as the gastrointestinal tract and blood-forming organs. Through further research, it was determined in 1935 that the mustard gas could inhibit the growth of chemically induced tumors in animals. Unfortunately, it was not known whether or not the toxic gas would kill the animal before it killed the tumor. Thus, Alfred Gilman and Louise Goodman conducted animal studies to investigate the toxicity and

pharmacokinetics of the gas and showed that it could significantly lessen lymphoma in mice [1]. The potential impact of chemotherapy to anti-cancer applications was then solidified to the scientific community and used in practice.

Chemotherapeutic agents are administered to patients at moderate to severe toxicities. The toxic hazards of chemotherapy are generally tolerated because of the belief that the higher the dose given, the more likelihood there is a favourable therapeutic response. The major life-threatening toxicities that a patient may exhibit include: gastrointestinal, bone marrow, hepatic, renal, cardiovascular, neuromuscular and respiratory toxicities. Other toxicities that are non-life-threatening but can affect the quality of life include nausea, vomiting and alopecia [1].

There are several ways to classify anti-cancer agents as some agents also belong to more than one group. The classes of anti-cancer agents include [1,2,3]:

- alkylating agents
    - platinum-based anti-cancer drugs
    - bioreductive alkylators
    - anthracyclines
    - topoisomerase inhibitors
- antimetabolites
- tubulin-interactive drugs

1.2.1: Alkylating Agents

Alkylating agents are those that interact with DNA, RNA or proteins by forming covalent chemical adducts [2]; however, it is commonly believed that DNA is the most important target for alkylating agents. Alkylation of these biological molecules may occur when the

electrophilic agent reacts covalently with their nucleophilic atoms; for example, amino, carboxyl, phosphate and sulfhydryl groups in nucleic acids, proteins, amino acids or glutathione. Since the nitrogen atom at the 7-position in guanine is highly nucleophilic, it is believed to be the main target for alkylation by nitrogen mustards as well as cisplatin [5].

Alkylation of DNA molecules can have biochemical and cellular consequences such as activation of enzymatic DNA repair processes, which can lead to single-strand breaks if there is a failed attempt at DNA repair. The two strands of the DNA helix may also become cross-linked by covalent reaction of the alkylator with two bases either on the same or opposite strands, which correspond to intra- and interstrand cross-linking, respectively. Alkylators may also alter the DNA base structures, which can cause miscoding during the replication process and lead to genetic mutations. These interactions with alkylators can effectively lead to cell death. Alkylating agents may be classified further as platinum-based, anthracyclines, bioreductive alkylators, or topoisomerase inhibitors [2].

1.2.1.1: Platinum-Based Drugs

Platinum-based anti-cancer drugs have been greatly investigated. Other metal-based compounds have also been synthesized and tested such as mercury and gold, but platinum-based compounds have shown the greatest success. The first prototype was cisplatin, which was discovered by accident in 1965 by Dr. Barnett Rosenberg [6]. Rosenberg was interested in the effects of electric fields on the growth of bacteria. His experimental setup consisted of two platinum electrodes, in which he assumed were inert, a water bath and *E.coli*. Remarkably, he observed that the growth of *E.coli* was greatly

inhibited. Further analysis and testing confirmed that it was the formation of cisplatin from the platinum electrodes that was responsible for this inhibition of growth. Fortunately, Rosenberg realized the potential of cisplatin in cancer therapy. Today, cisplatin is one of the most widely-used chemotherapeutic drugs. Other cisplatin analogs have been derived and tested, including carboplatin and oxaliplatin. The trans-isomer, transplatin, has also been tested, but has not been found to be therapeutically effective [1,2,3]. Cisplatin will be discussed in more detail in Section 1.4.

1.2.1.2: Anthracyclines

The mechanism of action of anthracyclines on cancer cells is controversial. The compounds may: 1) intercalate into DNA to inhibit the synthesis of macromolecules, 2) form oxidative free radicals that can damage DNA or be involved in lipid peroxidation, 3) bind and alkylate the DNA, 4) cross-link with the DNA, 5) interfere with the DNA unwinding or DNA strand separation and helicase activity, 6) affect the lipid membrane, 7) inhibit topoisomerase II activity to damage DNA and 8) induce apoptosis in response to topoisomerase II inhibition [7]. These compounds appear to be more toxic to cycling cells than resting cells [1,2,3]. The most common anthracyclines are daunorubicin, doxorubicin (marketed as Adriamycin) and epirubicin.

1.2.1.3: Topoisomerase II Inhibitors

Topoisomerase I and II are enzymes that break and rejoin one or both strands of DNA molecules, respectively. It is thought that topoisomerase II is the more important biochemical target compared to topoisomerase I. Topoisomerase II is able to form a temporary gate through both strands of DNA molecules so that one double-strand DNA

segment can pass through another. Topoisomerase II inhibitors bind to and trap the covalent complex formed between DNA and the topoisomerase. This effectively causes the formation of protein-associated single- or double-strand DNA breaks. Interestingly, free radicals can also be formed, which can damage DNA and other macromolecules. These complexes also block other important processes like DNA replication, which can lead to cell death [2]. Some anthracyclines such as doxorubicin are also considered to be topoisomerase II inhibitors. Other topoisomerase inhibitors include camptothecin and etoposide [1,2,3].

1.2.1.4: Bioreductive Agents

One main characteristic of tumor cells is their hypoxic environment (lacking oxygen). In the early 1950s, Gray et al. exploited the fact that hypoxia reduces the effectiveness of radiation treatments [8,9]. In fact, tumor cells with low oxygen levels are up to three times more resistant to radiation than those containing oxygen. In the early 1970s, Sartorelli et al. proposed the use of a prodrug to target the tumor cells in the hypoxic environment [10]. The prodrug can be made so that it is metabolized to a cytotoxic compound only in hypoxic cells; otherwise, it would be inactive and would not cause any or very little systemic toxicity.

Bioreductive drugs may also enhance the effects of radiation and standard chemotherapeutic drugs since bioreductive drugs are predominantly specific to hypoxic cells and radiation and chemotherapeutic drugs are more effective at killing aerobic cells. In order for bioreductive drugs to be effective, the tumor needs to be hypoxic and there needs to be an enzyme(s) that is able to reduce the drug to its cytotoxic counterpart [8].

The leading bioreductive agent is tirapazamine (TPZ, 3-amino-1,2,4-benzotriazine 1,4-dioxide), a heteroaromatic n-oxide compound [11]. Not only does it exhibit excellent hypoxia-selective cytotoxicities, but it has been shown that it can greatly enhance the efficacies of radiotherapy as well in combination with various chemotherapeutic agents *in vivo*, including cisplatin, cyclophosphamide, etoposide, bleomycin, doxorubicin, carboplatin, paclitaxel and 5-FU [12]. Its cytotoxic action is attributed to the one-electron reduction by cytochrome P450, P450R and nitric oxide synthase [13,14], generating a nitroxide radical intermediate. In the presence of oxygen, the intermediate back-oxidizes to the non-cytotoxic parent compound. In the absence of oxygen, the loss of water causes the radical intermediate to form an oxidizing radical that is able to cause DNA damage through hydrogen abstraction [15]. TPZ does not exhibit any bystander effects since the one-electron product is short-lived. Unlike other bioreductive agents, TPZ also has cytotoxicities at intermediate oxygen levels; in other words, TPZ is also able to target cells that are radioresistant but are not quite hypoxic for other bioreductive drugs to act upon [16]. Since the cytotoxic radical is short-lived, this broadened oxygen selectivity can be beneficial. On the contrary, the reduction of TPZ to its cytotoxic radical at intermediate oxygen tensions could prevent it from being delivered to chronically hypoxic tumor cells [17]. Thus, others have suggested that TPZ analogues be derived with improved diffusion characteristics [18,19,20].

1.2.2: Antimetabolites

Antimetabolites mimic metabolites that are important in the functioning of the biosynthesis of nucleic acids. Because they are chemically similar to endogenous metabolites, they use similar cellular uptake mechanisms and metabolic pathways, but

due to small differences in their structures, antimetabolites can disrupt nucleic acid synthesis. Key enzymes may be inhibited or cellular function may be altered after the antimetabolites are incorporated into RNA or DNA. Typically, antimetabolites affect cells in the S phase of the cell cycle since they disrupt nucleic acid synthesis. The most common antimetabolite, 5-Fluorouracil (5-FU), is a fluoropyrimidine antimetabolite that metabolically activates to fluorodeoxyuridine monophosphate (FdUMP), which inhibits thymidylate synthetase. It is then activated to fluorouridine triphosphate (FUTP), which is able to incorporate into RNA molecules. Gemcitabine (2',2'-Difluorodeoxycytidine) is also another common antimetabolite. After cellular uptake, the active metabolite (gemcitabine triphosphate) inhibits DNA chain elongation, which can lead to DNA fragmentation and thus, cell death [21].

1.2.3: Tubulin-Interacting Agents

Tubulin is a protein that polymerizes to form cellular microtubules, which are structural units involved in the formation of mitotic spindles during mitosis. Vinca alkaloids such as vincristine and vinblastine bind to tubulin, which inhibits microtubule formation and effectively prevents the cell from dividing. Although the antitumor effects are primarily from the interaction with tubulin, other biochemical effects include the inhibition of RNA and DNA synthesis. Taxanes such as paclitaxel (docetaxel) also interact with tubulin molecules, but unlike the vinca alkaloids, paclitaxel overstabilizes the microtubules instead of inhibiting their assembly [2,22]. It has also been reported that paclitaxel can cause cell cycle arrest in the G2/M phase [22].

Section 1.3: Combinational Chemotherapy

One method to limit the lethal toxicity of anti-cancer drugs while maintaining the highest therapeutic effect is by giving drugs in combination. Although the toxic effects are spread amongst different organs and there is a wider range of side effects, the lethal effects are minimized. One objective of administering drugs in combination is that the combined effect of the drugs is synergistic (greater than additive). The widely-accepted criteria used to design combinational drug regimens is the following [1,2,3]:

- Each drug should be active when used alone
- Drugs should have different mechanisms of antitumor action
- The toxic side effects of the drugs should not overlap so that each drug can be given at or near their maximum tolerated dose
- Drugs should have different resistance profiles
- Drugs may target different cell cycle phases

As will be shown in this work, this criterion is not necessary to form an effective drug regimen. In fact, this criterion should *not* be followed if one desires to design a regimen where one drug can synergistically potentiate the action of another. Even up until now, drug regimens are being designed using this criterion – this may be one main reason why many combinations have failed and even those that are clinically used do not produce satisfactory clinical outcomes.

There are many combinational therapy regimens available, depending on the type of cancer being treated, as well as the stage of the cancer. Typically, it requires many years for a certain regimen to become a gold standard for a specific type of cancer since

many clinical trials must be conducted to determine what the side effects are as well as the safe levels of dosages.

Combinational chemotherapy has been found to be far more superior than single-agent therapy in many types of cancer; for example, the response rates and overall survival rates of breast cancer patients have been greatly improved. The prognosis of these patients has been greatly increased with the introduction of anthracycline-based chemotherapeutic combinations [23]. A well-established regimen is FEC (5-FU + epirubicin + cyclophosphamide), which is commonly used to treat patients with both early- and late-stage breast cancer [23,24,25]. The FEC regimen has produced response rates of approximately 50% [23], with epirubicin being considered as the main contributor to the cytotoxic treatment of metastatic breast cancer. The FAC (5-FU + doxorubicin + cyclophosphamide) regimen is also commonly used to treat breast cancer patients since epirubicin and doxorubicin are structural analogs [23]. The FAC regimen also produced some efficacy (response rate of 35%) in the treatment of advanced pancreatic cancer, although the responses were short-lived and often not complete [26].

In hopes of finding a combination regimen that would be more effective than the FEC combination but without any additional toxicities, the gemcitabine, epirubicin and paclitaxel (GET) regimen was tested on patients with metastatic breast cancer [23,27]. This combination was formed from previous phase II studies that showed gemcitabine having high efficacy towards metastatic breast cancer patients [28]. A phase II study of the GET regimen showed promising results (response rates of 92%) [29]. On the contrary, a multicenter phase III study conducted by the Central European Cooperative

Oncology Group showed that the GET regimen is not superior to the FEC regimen in metastatic breast cancer patients [23].

5-FU is also used in combination with doxorubicin for patients with advanced pancreatic cancer [26,30]; however, there is no significant improvement in the survival of the patients and many patients experience greater toxic side effects [30]. These findings are similar for metastatic pancreatic cancer patients treated with 5-FU, doxorubicin and cisplatin. A phase II clinical trial done in 1991 observed a response rate of only 15% for non-pretreated patients, which was also accompanied by severe gastrointestinal toxicities [26].

Section 1.4: Cisplatin

Since its approval by the FDA in 1978, cis-diamminedichloroplatinum (II) (also known as cisplatinum, cisplatin or CDDP) has become one of the most widely used anti-cancer drugs in the world, particularly in testicular, bladder, ovarian and head and neck cancers. It is not surprising that most standard combinational chemotherapeutic regimens contain CDDP or one of its analogue agents. Despite its wide usage, CDDP suffers from severe toxicities and drug resistance (both intrinsic and acquired). Other platinum analogs such as carboplatin and oxaliplatin have also been derived to reduce the toxicities of CDDP, yet they have not shown such high efficacies as CDDP [1,2,3]. The chemical structure of CDDP is shown in Figure 1.1.

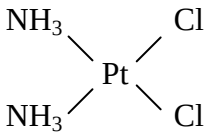

Figure 1.1: Chemical structure of CDDP

Immense efforts have been put forth to gain a deeper understanding of CDDP's mechanism of action. In the intracellular environment, the Cl-Pt bonds are broken in one or two steps, forming *cis*-$Pt(NH_3)_2$ as the end product that can react with DNA, RNA or protein molecules to form cross-linked species [1,2,3,31,32,33]. Although CDDP can react with various cellular components, DNA is considered to be the therapeutic target. These cross-links produce severe distortions in DNA and can lead to unwinding and kinking of the DNA strands. Both interstrand as well as intrastrand cross-links can be formed, but the majority of the adducts are 1,2-d(GpG) (approximately 65% of adducts) and 1,2-d(ApG) (about 25% of adducts) cross-links formed between neighbouring purine bases [31,32]. The bending of double-stranded DNA due to the formed 1,2-intrastrand *cis*–[$Pt(NH_3)_2$-d(GpG)] cross-link has been shown in solution by nuclear magnetic resonance and X-ray crystallography studies [34,35].

Section 1.5: A New Reaction Mechanism of Action

Although many postulates have been made about the cytotoxic mechanisms of CDDP, these are usually only made on the cellular level. In order to improve cancer therapies

with CDDP, the cytotoxic mechanisms need to be understood on a molecular level. The most widely-accepted theory is that the chloride atoms are displaced by water molecules (aquation), producing the reactive aqua complexes – the majority being $[PtCl(H_2O)\text{-}(NH_3)_2]^+$ [1,2,3,31,32,33].

This widely-accepted hydrolysis reaction of CDDP to form DNA adducts has been challenged by Lu et al. [32,33]. Lu reasoned that this hydrolysis reaction is highly unlikely to result in the chlorine-bond break when CDDP reacts with DNA. Firstly, since the most cytotoxic adduct is attributed to the 1,2-d(GpG) cross-link, a species is required to bind to two neighbouring guanine bases. In the hydrolysis of CDDP, it is most likely the $[Pt(H_2O)_2\text{-}(NH_3)_2]^{2+}$ that can bind to two neighbouring guanine bases; however, there has been evidence that under physiological conditions, this complex is the least likely to form [36,37]. Also, the reaction rate constant for the hydrolysis of CDDP has been estimated to only be approximately 10^{-4} $M^{-1}s^{-1}$ [36]. Furthermore, this was estimated in low chlorine concentrations and in the presence of solvents ($HClO_4$ and $NaClO_4$) at 45^oC; therefore, this reaction rate constant is even lower under physiological conditions (at 37^oC in an environment containing mostly water).

It is long known that halogen-containing molecules have extremely efficient dissociative attachment reactions with low-energy electrons [38-41]. This reaction can produce a halogen anion and a neutral radical. Interestingly, Lu and Madey [42] discovered that these electron-induced reactions are largely enhanced by the presence of NH_3-containing molecules. The dissociative electron transfer mechanism proposed by Lu and Madey [42] and Lu and Sanche [43] is the following:

$$e^-:(NH_3)_n + ABCl_x \rightarrow [ABCl_x]^{*-} \rightarrow Cl^- + ABCl_{x-1}^{\bullet}$$

where $ABCl_x$ is a chlorine-containing molecule and $e^-:(NH_3)_n$ is a presolvated electron that is localized in the small polar molecular cluster. From this dissociative electron transfer mechanism, Lu predicted that CDDP can have very efficient dissociative attachment reactions with weakly-bound electrons because it is a small molecule that contains both NH_3 and chlorine groups.

Using time-resolved pump-probe femtosecond laser spectroscopy, Lu and co-workers discovered the high reactivity of CDDP with weakly-bound prehydrated electrons (precursor of the solvated electron) generated in radiotherapy [33], as well as the preferential electron transfer reaction of CDDP with the guanine base [32]. In the first case, weakly-bound electrons were generated by two-UV-photon excitation of water molecules. The following electron transfer reaction between the prehydrated electrons and CDDP was monitored:

$$e_p^- + Pt(NH_3)_2Cl_2 \rightarrow [Pt(NH_3)_2Cl_2]^{*-} \rightarrow Pt(NH_3)_2Cl^{\bullet} + Cl^-$$

$$e_p^- + Pt(NH_3)_2Cl \rightarrow [Pt(NH_3)_2Cl]^{*-} \rightarrow Pt(NH_3)_2^{\bullet} + Cl^-$$

In the second case, Lu et al. demonstrated that in chemotherapy, CDDP preferentially reacts with guanine bases by capturing two electrons from two neighbouring guanine bases [32]. This is reasonable, since guanine is the most thermodynamically favoured electron donor compared to the other three DNA bases. Thus, it was determined that the release of chlorine atoms and the binding of $Pt(NH_3)_2$ to DNA is due to the electron

transfer reaction between the intact CDDP and the guanine bases, which is enhanced by the NH_3 groups. Interestingly, Lu also observed the strong electron transfer reaction between ground-state CDDP and a weakly-bound electron donor [33]. Furthermore, enhanced DNA damage was observed when a tiny electron source was produced in DNA-CDDP solution [33]. These femtosecond time-resolved laser spectroscopic studies provide a deep understanding of the molecular mechanisms of action of CDDP used in chemotherapy and in combination with radiotherapy or another chemical agent.

Section 1.6: Combinational Chemotherapy with Cisplatin

Due to its high efficacy in single-agent chemotherapy, it is not uncommon to have a patient treated with a CDDP-containing combinational chemotherapeutic regimen. For example, a phase III randomized trial published in 1992 [44] compared CDDP and 5-FU as single agents and in combination for advanced squamous cell carcinoma of the head and neck. The overall response rate of the CDDP and 5-FU combination was 32%, whereas those for CDDP or 5-FU alone were 17% and 13%, respectively. Unfortunately, patients treated with the combination experienced higher toxicities. Thus, although the response rate was higher for the combination compared to the single agents, the survival rates did not improve.

Several groups have demonstrated the anti-cancer activity of paclitaxel given alone against ovarian carcinoma, breast carcinoma, lung carcinoma, melanoma and head

and neck cancer [45,46]. Due to paclitaxel's broad activity with different human cancers, especially CDDP-sensitive tumors, the paclitaxel and CDDP combination has become one of the most commonly used paclitaxel-based chemotherapeutic regimens for solid tumors [46]. In preclinical studies, this combination has even shown synergistic interactions in a schedule-dependent manner [22,47,48]. Jekunen et al. [48] showed the schedule-dependent synergistic interaction of paclitaxel with CDDP in human ovarian carcinoma 2008 cells *in vitro.* Interestingly, this combination was highly synergistic for cells treated with paclitaxel first, and then CDDP; however, when this sequence was reversed, they observed an antagonistic interaction. These *in vitro* observations suggest the clinical efficacy of this drug combination, but they were unable to identify the mechanism responsible for the synergistic interaction between CDDP and paclitaxel. Vanhoefer et al. [22] also made similar observations for human gastric and ovarian carcinoma cell lines, where the combination was found to be either additive or synergistic when paclitaxel was given before CDDP. The antagonistic effects observed for the reversed sequence was attributed to the CDDP-induced cell cycle effects since paclitaxel also affects the cell cycle (causes a G2/M-interphase blockade), or CDDP-induced alterations in the specific or non-specific binding sites of paclitaxel (tubulin).

Clinical studies have shown conflicting results for the paclitaxel-CDDP combination. For example, a phase II study of women with clinically CDDP-resistant ovarian cancer who were treated with only paclitaxel only had a response rate of 37% [49]. Strikingly, a study done in 1996 by McGuire et al. then showed that the CDDP-paclitaxel combination can induce a response rate of 73% in advanced ovarian carcinoma patients [50]. A phase II trial in 2000 [51] showed activity in patients with advanced

esophagus carcinoma who were treated with paclitaxel and CDDP; however, the group was not able to recommend the combination tested due to severe toxicities induced on patients. Fifty percent of patients were hospitalized for toxicity and 11% died from therapy-related complications. Thus, the therapeutic efficacy of the paclitaxel-CDDP combination is dependent on the cancer-type [50,51].

As a single agent, gemcitabine has been shown to have activity against metastatic non-small-cell lung cancer, ovarian carcinoma, cervical cancer and head and neck squamous cell carcinoma [52-54]. These tumors are also commonly treated with CDDP. Due to their differences in toxicity profiles and their predicted mechanisms of action, the gemcitabine-CDDP combination has been suggested [53,54]. Thus, this chemotherapeutic regimen is one of the most widely-used in clinic in different types of cancers including bladder cancer, relapsed breast cancer and pancreatic cancer [30]. Both *in vitro* and *in vivo* data have suggested that gemcitabine in combination with CDDP can provide synergistic interactions if given at the appropriate schedule [21,52,53,54]. This synergistic action may be attributed to gemcitabine's ability to inhibit the removal of CDDP-induced DNA interstrand cross-links [21,56]. Using Chinese hamster ovary cell lines deficient in the different DNA repair pathways (base excision repair, nucleotide excision repair, homologous recombination and non-homologous end joining), Crul et al. [54] suggested that this synergistic interaction between the two drugs may be related to homologous recombination of damaged DNA.

In a phase II study in 2002 [21], patients exhibiting metastatic or recurrent nasopharyngeal carcinoma were treated with gemcitabine and CDDP. The gemcitabine-CDDP combination regimen achieved a high response rate of 78%, where 22% of

patients had complete responses, despite half of the patients being previously treated with prior chemotherapy or radiotherapy. Patients exhibited only moderate toxicity levels, which were considered relatively safe. The gemcitabine-CDDP combination regimen was also studied in previously non-treated patients with advanced non-small cell lung cancer [52]. The combination induced a high response rate (54%) and produced only modest side effects that were only short-lived.

Unfortunately, results in a 2008 phase II study were not as promising [57]. The clinical activity and toxic tolerability of the gemicitabine-CDDP combination was evaluated in chemo-naïve advanced hepatocellular (liver) carcinoma. The trial was stopped early due to the lack of efficacy of the drug combination. Progression-free survival and overall survival rates were very short; therefore, this group was not able to recommend further studies for the gemcitabine-CDDP combination to treat advanced hepatocellular cancer patients.

The bioreductive drug tirapazamine (TPZ) has been shown to enhance the response rates *in vitro* when added to CDDP in certain cell lines. Incubation of cells with TPZ and CDDP together under hypoxia increases CDDP-induced DNA interstrand cross-links, which suggests that TPZ inhibits or delays repair of the DNA cross-links. Although this combination is still undergoing clinical trials, the molecular mechanism of the TPZ-CDDP interaction is still unclear and inconclusive due to inconsistent results from various research groups. In fact, Phase III clinical trials have been disappointing; TPZ was found to introduce additional toxic side effects [19,20]. This is a clear example of the use of the classical criterion used to design combinational chemotherapeutic drug regimens, where both drugs (TPZ and CDDP) have their own antitumor actions. It is

clear that the mechanisms underlying the cytotoxicities of TPZ are still not understood, as manifested through the poor outcomes in late clinical trials [16,17,19,20].

Although the response rates for CDDP-containing regimens are relatively high, patients still experience extremely high levels of toxicity that are sometimes lethal. In fact, some trials have been stopped due to toxic-related deaths [58]. In order to prevent lethal events from occurring, in depth studies need to be performed to study the reaction mechanisms between drug combinations.

Section 1.7: Motivation and Research Goals

The work by Lu and co-workers has motivated this combinational chemotherapy study, where an electron-donating molecular promoter, namely N, N, N', N'-Tetramethyl-p-phenylenediamine (referred to as PM2A in this thesis), is used to enhance the therapeutic efficacy of CDDP. PM2A is a well-known biochemical electron donor used in biological systems [59]. It is hoped that this modulation by PM2A will result in synergetic effects in combination with CDDP. As a result of improved CDDP activities, lower CDDP dosages may be used in the clinic; thus, this may greatly reduce the toxic side effects that patients experience, effectively improving the prognosis of cancer patients treated with CDDP.

To test and measure the synergistic effects between PM2A and CDDP, *in vitro* methods were performed on HeLa cells (a cervical cancer cell line) and results presented in the following chapters.

The structure of this thesis is organized as the following. This chapter gives an introduction on cancer chemotherapy, cisplatin and our research goals. Chapter 2 gives an overview of the biological concepts touched upon in this thesis, including cancer, apoptosis and the cell cycle. In Chapter 3, the results of the MTT assay are presented, which show the effects of the drug regimen on cell survival rates. Chapter 4 presents images using fluorescence microscopy, which are used to visualize the changes in the cell morphologies as a result of the PM2A-CDDP combination. In Chapter 5, flow cytometric studies are shown to observe the changes in the cell cycle perturbations. Flow cytometry is also utilized to show the increase in the amount of fragmented genomic DNA, as presented in Chapter 6. In Chapter 7, an absorption spectroscopic study is utilized to show the electron-transfer reaction of PM2A with CDDP. Finally, the conclusions are given in Chapter 8.

Chapter 2. Biological Background

Section 2.1: Cancer

Cancer occurs when the cell loses its ability to control and regulate its proliferation, differentiation and programmed cell death processes. Most cancers will result in the development of a solid tumor due to their failure to respond to homeostatic control mechanisms [4,78].

The cause of cancer lies in the abnormalities of the cell's genetic material. These abnormalities may be caused by carcinogens such as radiation or chemicals. Genetic abnormalities may also be inherited from birth, or may occur randomly in processes like DNA replication. Even if cellular machinery is unable to repair the genetic abnormalities, cancerous cells will still proceed to replicate their erroneous DNA, whereas normal cells will undergo programmed cell death (also known as apoptosis) to prevent themselves from being replicated [60].

Hanahan and Weinberg [78] suggested that most human tumors exhibit the following physiological characteristics that allow them to become malignant: self-sufficiency in growth signals, insensitivity to growth-inhibitory signals, evasion of programmed cell death, limitless replicative potential, sustained angiogenesis and tissue invasion and metastasis.

Section 2.2: The Cell Cycle

The cell goes through the cell cycle in cell proliferation, where its DNA is replicated and the replicated chromosomes are segregated, thus dividing the original cell into two daughter cells. Cell division consists of interphase, where the cell replicates its DNA, and mitosis (M), where the cell physically divides. Interphase is composed of the GAP1 (G1), S and GAP2 (G2) phases. The cell first prepares to replicate its DNA in the G1 phase. It may choose to go into the dormant G0 phase, where the cell is in a resting state (non-growing and non-proliferating). After the G1 phase, the cell then starts to replicate its DNA in the S phase of the cell cycle. In the G2 phase, RNA and proteins are produced and the cell starts to prepare for mitosis [30,61]. The cell cycle is shown in Figure 2.1.

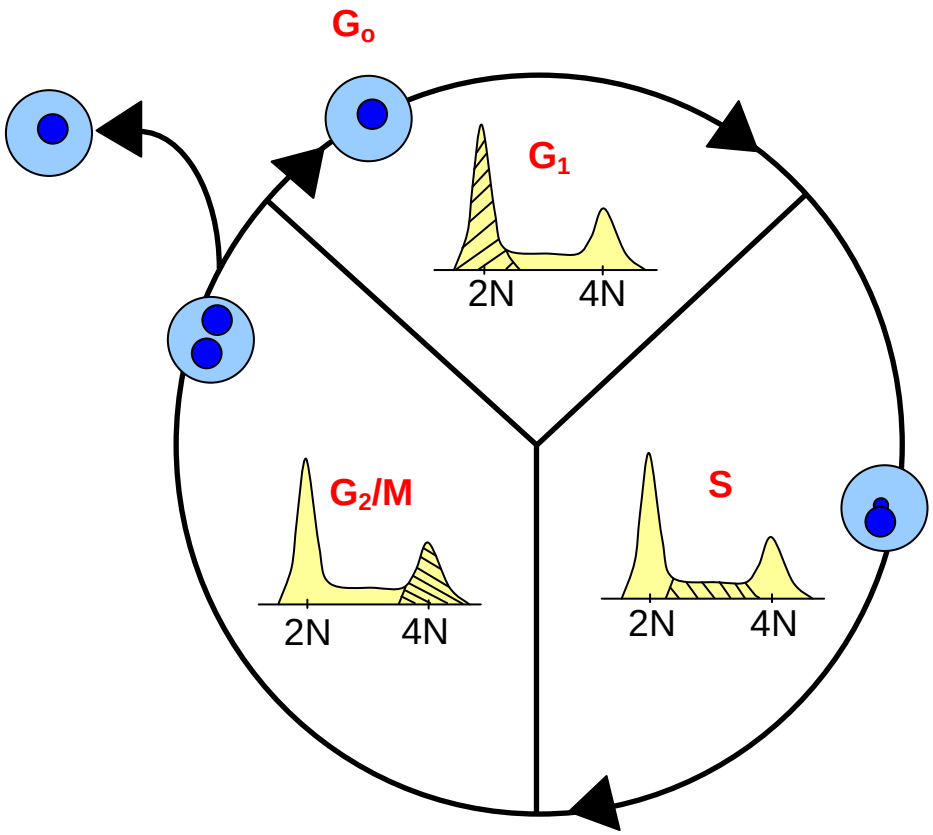

Figure 2.1: Schematic of the cell cycle phases in cell division

To maintain the integrity of the host organism, apoptosis and cell proliferation need to be tightly regulated to eliminate cells that are proliferating abnormally. For this reason, apoptosis and proliferation are tightly coupled. Cell cycle checkpoints occur in the G1/S phase boundary and also in the G2/M phase boundary [62,63]. These checkpoints ensure that cell cycle events occur in order, and also that critical events within a particular phase are completed before the cell proceeds to the next cell cycle phase; thus, this prevents the formation of genetically abnormal cells. It is believed that arrest in the G1 phase prevents the replication of damaged DNA and arrest in the G2 phase prevents the cell from segregating defective chromosomes [64]. In response to stress on the intracellular or extracellular environments, such as genotoxic stress, the cell may arrest at a cell cycle checkpoint. For example, growth arrest may occur if cell cycle regulators detect DNA damage or if the chromosomes are misaligned on the mitotic spindle. At the cell cycle checkpoint, the cell may attempt to repair the damages. If successful, the cell will continue to progress through the cell cycle. But if the damage is too severe to be repaired, or if the cell fails to repair the DNA, the cell may undergo apoptosis to eliminate itself. However, cell cycle regulators in malignant cells may fail to determine which one of these options is suitable; for instance, the cell may not decide to undergo apoptosis in response to a cytotoxic drug [62]. Thus, it is desirable to search for drug compounds that can block cell cycle progression and induce growth arrest [63,79].

Section 2.3: Apoptosis

Apoptosis is a multistep process that is orchestrated by a specific sequence of events. The timing of each event depends on the type of cell and also the method of induction. Apoptosis is marked by the following order of events after induction: collapse of the mitochondrial transmembrane potential, caspase activation, externalization of phosphatidylserine in the plasma membrane, severe chromatin condensation (not to be confused with condensation during mitosis), DNA fragmentation and loss of plasma membrane integrity [60,65].

Apoptotic cells also exhibit hypersegmentation of nuclear chromatin of irregular size. These structures bud off from the cell surface and form “apoptotic bodies”. The late-stage DNA fragmentation of apoptotic cells, which leads to the disintegration of the nucleus, occurs due to the DNA cleavage at sites between nucleosomes at ~200-bp intervals. Fragmented DNA produce exposed 3’-OH ends, and thus can be detected using in situ assays such as the terminal deoxynucleotidyl transferase dUTP nick end labeling (TUNEL) method [66,67].

Chapter 3. Cell Survival Study Using the MTT Assay

Section 3.1: Introduction

To test the cytotoxic actions of drugs *in vitro*, the cell survival fraction is usually measured by counting the number of cells that either include or exclude a dye. One of the most common cell viability and proliferation assays used is the MTT assay developed by Mosmann in 1983 [68]. This method allows one to count the number of cells indirectly. It involves the conversion of yellow MTT (3-(4,5-dimethylthiazol-2-yl)-2,5-diphenyltetrazolium bromide) to insoluble purple formazan crystals by metabolically-active cells (live cells). The reduction of MTT occurs in the mitochondria of living cells, where the mitochondrial reductase enzymes are active. Using a solubilizing agent, the formazan crystals are dissolved and their absorbance measured, giving indication to the number of cells that survived. This is a quantitative method that is rapid in terms of the required drug treatment time as well as the total protocol time compared to the clonogenic assay, which measures cell survival on the long-term scale [69]. Typically, the MTT assay can be performed within several days, whereas the clonogenic assay can last 1-3 weeks. The clonogenic assay measures the ability of a single cell to grow into a colony (one colony is at least 50 cells) and is often used to study cells that are treated with ionizing radiation.

To evaluate the synergistic effects of PM2A in combination with CDDP on cell viability, the MTT assay was utilized.

Section 3.2: Materials and Methods

3.2.1: Cell culture and treatment

HeLa (cervical cancer cell line) cells were purchased from American Type Culture Collection. The medium for cell culture was minimum essential medium (MEM) with phenol red, which was supplemented with 10% fetal bovine serum (FBS), 100 units/mL penicillin G and 100 μg/mL streptomycin. CDDP (Sigma) was dissolved in ultrapure water and PM2A in pure ethanol, where the final concentration of ethanol was always less than 1% when treated to cells. Ultrapure water with a resistivity of >18.2 MΩ/cm was obtained using a NANOpure DIamond TOC Life Science ultrapure water system (Barnstead International). The cells were split every 3 days, or once they reached a confluency of ~85% in 25 cm^2 flasks. The cells were cultivated by first rinsing the cells twice with phosphate buffered saline (PBS), then trypsinizing for ~2-3 minutes and deactivating the trypsin by adding 2 mL of fresh medium. The cells were removed from the flask surface by gently washing with medium. The solution was then centrifuged at 100 *g* for 5 minutes using an Allegra X-22R Centrifuge (Beckman Coulter). The old medium was removed without disrupting the cell pellets, and then 1 mL of new medium was added to resuspend the cells by gently pipetting up and down. Approximately 20% of the solution containing the cells was then used to further cultivate the cells in 25 cm^2 flasks. Cells were always incubated at 37^oC and the CO_2 levels maintained at 5% in a Forma Series II Water Jacketed CO_2 Incubator (Thermo Electron Corporation).

3.2.2: Cell survival measurement by MTT

Cells were seeded in clear 96-well plates (5 x 10^3 cells/well) in triplicate for 24 h. The culture medium containing phenol red (200 μL/well) was replaced by new culture medium (200 μL/well) and treated for 24 h with varying drug concentrations in the CO_2 incubator (37^{o}C, 5% CO_2). After the drug treatment, cells were replaced with new medium (100 μL/well) containing 1.2 mM MTT in phosphate buffered saline (Sigma) and incubated for 4 h in the dark in the CO_2 incubator. The medium was then removed by inverting the microplate on paper towels and gently absorbing the medium. After removing any excess medium (containing phenol red), the formazan crystals were solubilized with 100 μL DMSO. After 10 minutes of shaking, the fraction of live cells was determined by measuring the absorbance at 540 nm using a UV/Vis Multiskan absorbance microplate reader (Thermo Scientific), which is directly proportional to the number of viable cells. The cell survival rates were calculated by dividing the absorbance values of the treated cells by the absorbance of the untreated control cells and multiplying by 100 to obtain the percentages. The cell survival rates were plotted against drug concentrations to obtain a dose-response plot.

Section 3.3: Results and Discussion

HeLa cells were treated with 0, 10, 20, 30, 40 and 50 μM CDDP with and without 100 μM PM2A for 24 h. As shown in Figure 3.1, 100 μM of PM2A provides the maximum dose having minimal cell-killing effects as a single agent. Figure 3.2 indicates that a 24 h

treatment with CDDP decreases the cell viability in a dose-dependent manner. Treatment with only 100 μM PM2A slightly decreases the cell viability compared to the untreated cells (85% cell survival rate compared to untreated control). Strikingly, the addition of 100 μM PM2A to CDDP greatly enhances the effects of CDDP in a synergistic manner, which is most prominent for concentrations greater than 20 μM CDDP. At 10 μM of CDDP, the cell survival rate decreased from 79% to 64% with the addition of 100 μM PM2A. At 20 μM CDDP, the cell survival rate decreased from 72% to 43% with the addition of 100 μM PM2A. At concentrations greater than 30 μM CDDP, the addition of PM2A killed most or all of the cells, where the absorbance is due to background residual formazan. For cells treated with 30 μM CDDP, the addition of 100 μM PM2A resulted in a decrease in cell survival rate from 58% to 16%. At 40 μM CDDP, the cell survival rate decreased from 44% to 11% with the addition of PM2A. Finally, a treatment of 50 μM CDDP had a decrease from 21% to 8% in cell survival with the addition of 100 μM PM2A.

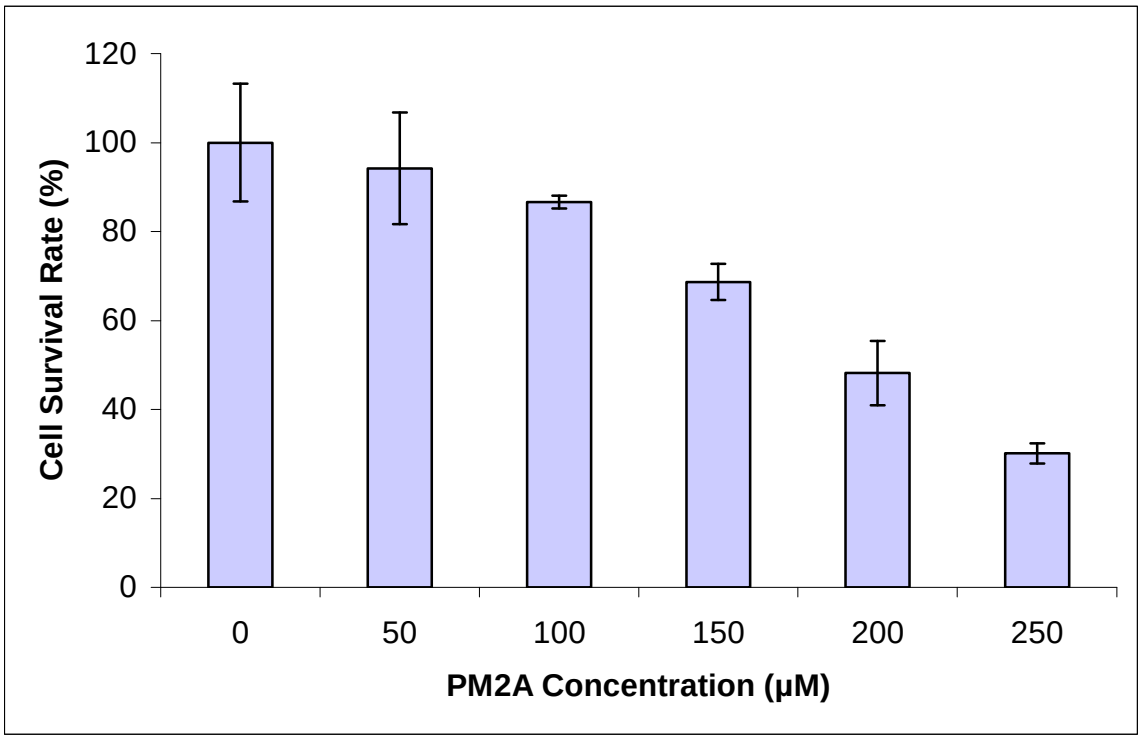

Figure 3.1: Cell survival rates for HeLa cells treated with 0 – 250 μM PM2A for 24 h.

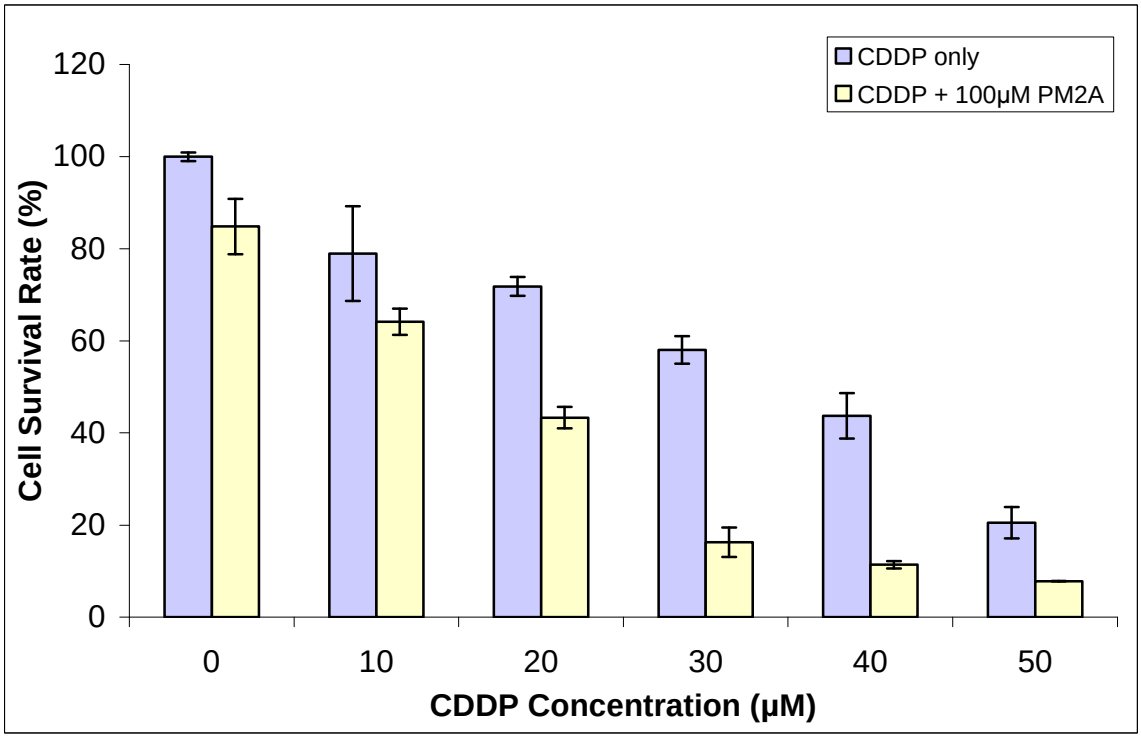

Figure 3.2: Cell survival rates for HeLa cells treated with 0 – 50 μM CDDP (± 100 μM PM2A) for 24 h.

Section 3.4: Conclusions

Although the cell-killing effects are not as obvious at lower concentrations of CDDP, it is predicted that these effects would be more prominent if the cells were treated for longer periods of time. It is possible that the cytotoxic effects of the combination regimen would be more obviously manifested at lower CDDP concentrations using an assay that probes long-term cell survival, such as the clonogenic assay. Differences in the cell survival rates between the single-agent therapy and combinational therapy might have been greater at larger CDDP concentrations (greater than 20 μM CDDP). This is likely due to the reason that to make the combination therapy effective, certain concentrations of both CDDP and PM2A must be present inside the cell or more effectively in the cell nucleus.

These MTT results suggest that although PM2A, alone, has minimal detrimental effects on HeLa cells, the cell-killing effects are significantly increased when the combination of PM2A + CDDP is used. This indicates that the effects are *synergistic* since the effects of the combination are greater than the sum of the single-agent effects, thus supporting this combination regimen as a viable one.

Chapter 4. Changes in Cell Morphology Using Fluorescence Microscopy

Section 4.1: Introduction

Many chemotherapeutic agents exert their cytotoxic effects by inducing programmed cell death, also known as apoptosis. The importance of apoptosis in the cell-killing actions of many drugs *in vitro* has been implicated, including etoposide, camptothecin, vincristine, paclitaxel, 5-FU and CDDP [70]. It has also been suggested that the disruption in the apoptotic response to CDDP can lead to resistance to CDDP [71]. Thus, it is reasonable to conclude that apoptosis is an imperative event in the cytotoxic effects of CDDP on cancer cells.

A landmark apoptotic event is the hypersegmentation of nuclear chromatin of irregular size. Apoptotic cells exhibit cell blebbing, resulting in the budding off of these structures from the cell surface; these are termed, “apoptotic bodies” [66,67]. This change in cell morphology can be observed using a nuclear stain and viewed using fluorescence microscopy. The stained nuclei would appear brighter due to the severe condensation of DNA.

Section 4.2: Materials and Methods

4.2.1: Cell culture and treatment

HeLa (cervical cancer cell line) cells were purchased from American Type Culture Collection. The medium for cell culture was minimum essential medium (MEM) with phenol red, which was supplemented with 10% fetal bovine serum (FBS), 100 units/mL penicillin G and 100 μg/mL streptomycin. CDDP (Sigma) was dissolved in ultrapure water and PM2A in pure ethanol, where the final concentration of ethanol was always less than 1% when treated to cells. Ultrapure water with a resistivity of >18.2 MΩ/cm was obtained using a NANOpure DIamond TOC Life Science ultrapure water system (Barnstead International). The cells were split every 3 days, or once they reached a confluency of ~85% in 25 cm^2 flasks. The cells were cultivated by first rinsing the cells twice with phosphate buffered saline (PBS), then trypsinizing for ~2-3 minutes and deactivating the trypsin by adding 2 mL of fresh medium. The cells were removed from the flask surface by gently washing with medium. The solution was then centrifuged at 100 *g* for 5 minutes using an Allegra X-22R Centrifuge (Beckman Coulter). The old medium was removed without disrupting the cell pellets, and then 1 mL of new medium was added to resuspend the cells by gently pipetting up and down. Approximately 20% of the solution containing the cells was then used to further cultivate the cells in 25 cm^2 flasks. Cells were always incubated at 37^oC and the CO_2 levels maintained at 5% in a Forma Series II Water Jacketed CO_2 Incubator (Thermo Electron Corporation).

4.2.2: Cell morphological changes by fluorescence microscopy

Cells were cultured in black 96-well plates (~5 x 10^3 cells/well) for 24 h. The culture medium (200 μL/well) was replaced by new culture medium (200 μL/well) and incubated in the CO_2 incubator (37^oC, 5% CO_2) for 11 h with 0, 15, 30 and 50 μM CDDP (± 100 μM PM2A). After the drug treatment, cells were gently washed once with PBS (while avoiding washing away floating cells) and stained with Hoechst 33342 for 12 minutes. The stain was removed and washed once with PBS, then the cells were fixed with 1% paraformaldehyde in methanol for 10 minutes and viewed under fluorescence using an Eclipse TS100 inverted microscope (Nikon Canada Inc.) and appropriate UV filters. Images were taken with a DS-Qi1Mc cooled digital camera (Nikon Canada Inc.).

Section 4.3: Results and Discussion

Representative fluorescent images of cells treated with different CDDP concentrations (with and without the addition of PM2A) for 11 h are shown in Figure 4.1(a-h). Figures 4.1 a) and b) show untreated cells (0 μM CDDP) and those treated with only 100 μM PM2A, respectively. Untreated HeLa cells had intact nuclei and did not exhibit condensation of nuclear material. The addition of 100 μM PM2A to untreated HeLa cells did not change the cell morphology. Cells treated with 15 μM CDDP without and with 100 μM PM2A (Figure 4.1 c) and d)) had only slight differences in cell morphology. In the cells treated with PM2A, we started to observe the formation of DNA condensation and apoptotic bodies, as seen by the bright spots in d) and indicated by the red arrows.

Cells treated with only 30 μM CDDP exhibited some apoptotic bodies at 11 h of drug treatment time (Figure 4.1 e)). With the addition of 100 μM PM2A (Figure 4.1 f)), there was some increase in the number of dead cells as indicated by the apoptotic bodies. A considerable amount of cells died when treated with 50 μM of CDDP for 11 h (Figure 4.1 g)). But with the addition of 100 μM PM2A, the number of dead cells and apoptotic bodies markedly increased, as seen in Figure 4.1 h). It is also interesting to note that there were actually more dead cells in the 50 μM CDDP + 100 μM PM2A group that are not visible in the image, but were washed away during the staining procedure, as made evident by the lower cell density compared to cells treated with only 50 μM CDDP.

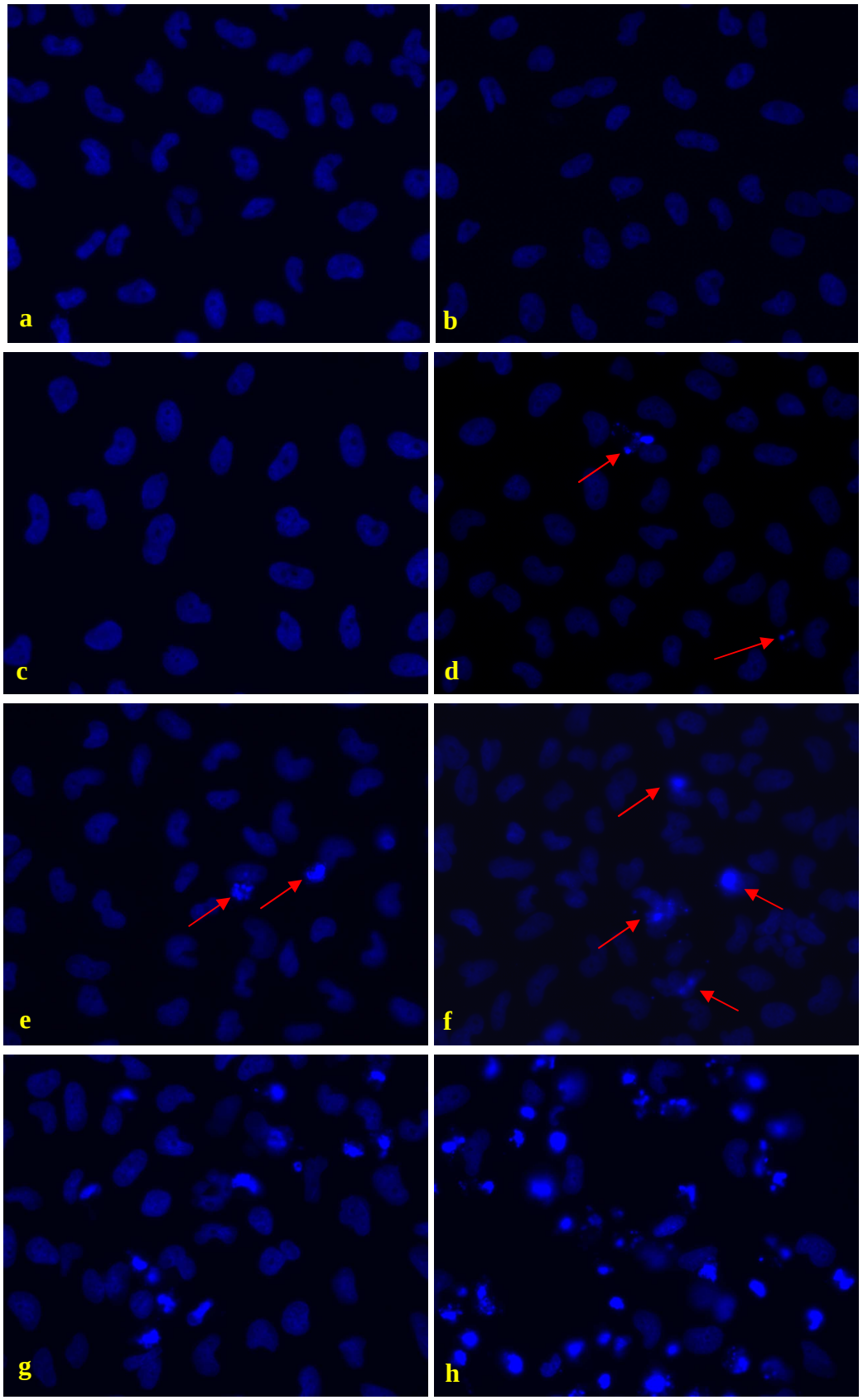

Figure 4.1: HeLa cells treated for 11 h and nuclear-stained with Hoechst 33342. a) 0 μM CDDP, b) 0 μM CDDP + 100 μM PM2A, c) 15 μM CDDP, d) 15 μM CDDP + 100 μM PM2A, e) 30 μM CDDP, f) 30 μM CDDP + 100 μM PM2A, g) 50 μM CDDP, h) 50 μM CDDP + 100 μM PM2A. Arrows in a-f indicate apoptotic cells, but not indicated in g-h.

Section 4.4: Conclusions

Obvious differences were seen between cells treated with high concentrations of only CDDP and CDDP + 100 μM PM2A. These differences were not very significant for cells treated with lower concentrations of CDDP (those that are clinically relevant) at 11 h, but it is expected that large differences for the lower concentrations would be observed when treated for longer periods of time.

The cell populations might have contained those that were necrotic (cell injury that can cause inflammation; “messy” death), although it was difficult to identify these cells by just staining with Hoechst. The cells can be incubated with a cell-impermeable stain; necrotic cells would be stained based on the assumption that the plasma membrane of necrotic cells are permeable. But the user must be cautious in that the plasma membrane of *late* apoptotic cells also lose their integrity. Therefore, an optimum time-window to detect this would be early in the apoptotic phase, such that markers like caspases are activated.

Thus, the efficacy of the PM2A-CDDP combination is supported by the enhancement in the number of apoptotic cells compared to the treatment with the single agents.

Chapter 5. Cell Cycle Analysis by Flow Cytometry

Section 5.1: Introduction

It is commonly believed that exposure of cells to CDDP can cause inhibition of DNA synthesis and therefore, signal the cell to undergo cell death [31,34]. It has also been proposed that CDDP exhibits its cytotoxic effects by triggering G2 cell cycle arrest and apoptosis [31,72,73]. At cell cycle checkpoints, DNA lesions may be “sensed”; failure to overcome this blockage can lead to cell death [79]. The cytotoxicity of CDDP appears to be cell cycle phase independent, but some types of cells may be more sensitive to CDDP in the G1 phase [2].

To analyze the cell cycle progression and the effects of a drug regimen on the cell cycle, one can use flow cytometry to quantify the DNA content. In cell cycle analysis, DNA of all cells in the sample are stained by a fluorescent DNA-binding agent such as propidium iodide. By noting that cells in the G1 phase have one copy of the DNA and two copies in the G2/M phase, the cell population in each phase of the cell cycle can be determined. Cells in the S phase exhibit between one and two copies of DNA. If the cells are fixed and permeabilized, cells that have fragmented DNA will have less than one copy of DNA since the fragmented DNA can escape out of the cells through the porous membrane; these are denoted as the sub-G1 fraction and can be attributed to cells that have undergone apoptosis. Counting the number of cells having specific amounts of DNA would generate a histogram similar to that in Figure 5.1. Cells in the G1 phase would exhibit a certain fluorescent intensity, whereas cells in the G2/M phase would have

double this intensity. Cells in the S-phase would have intensities between those of G1 and G2/M, and cells in the sub-G1 fraction have intensities less than that of the G1 fraction [74]. For instance, the G1 cells are located at 200 on the DNA Content axis of Figure 5.1, G2/M cells at 400, S phase cells in between 200 and 400 and the sub-G1 cells at less than 200. The broad peaks seen in the histogram depend on the resolution of the flow cytometer as well as the levels of variability in the sample population [74].

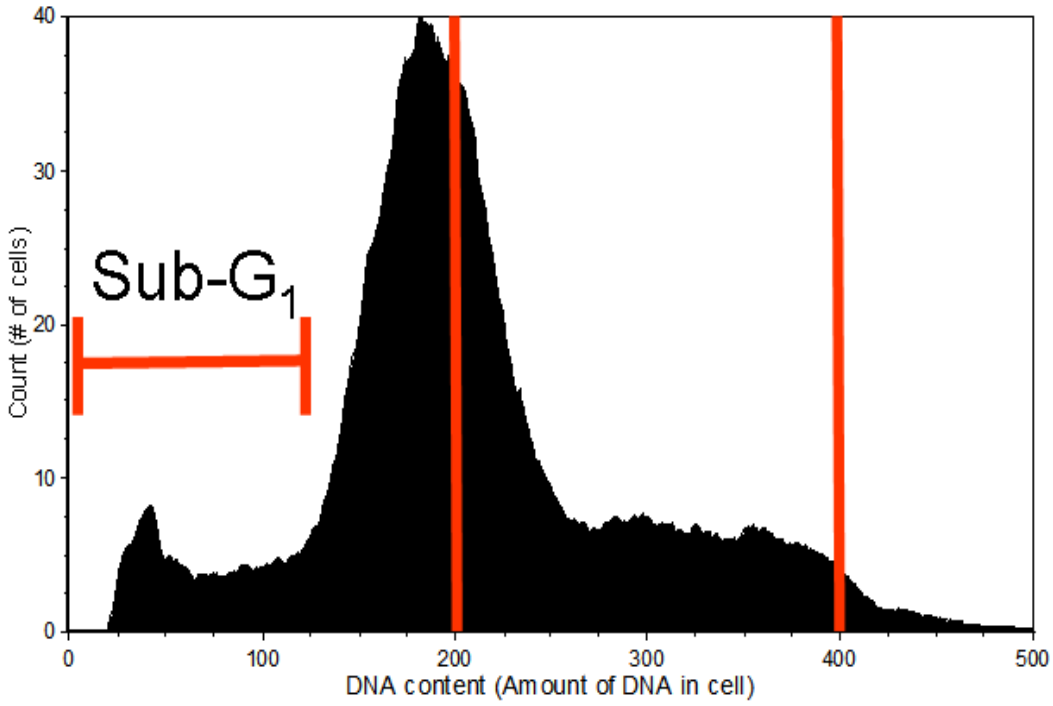

Figure 5.1: Sample DNA histogram for cell cycle analysis

The cell cycle progression can be analyzed over time to observe where in the cycle the cells accumulate. This may provide information on the action of a drug regimen and if applicable, which part of the cell cycle the cells are most sensitive to the drug. This information is usually cell- and stress-specific. For example, Yamada and Puck observed

that low-dose X-irradiation of HeLa cells can lead to a dose-dependent arrest in the G2 phase [75].

Section 5.2: Materials and Methods

5.2.1: Cell culture and treatment

HeLa (cervical cancer cell line) cells were purchased from American Type Culture Collection. The medium for cell culture was minimum essential medium (MEM) with phenol red, which was supplemented with 10% fetal bovine serum (FBS), 100 units/mL penicillin G and 100 μg/mL streptomycin. CDDP (Sigma) was dissolved in ultrapure water and PM2A in pure ethanol, where the final concentration of ethanol was always less than 1% when treated to cells. Ultrapure water with a resistivity of >18.2 MΩ/cm was obtained using a NANOpure DIamond TOC Life Science ultrapure water system (Barnstead International). The cells were split every 3 days, or once they reached a confluency of ~85% in 25 cm^2 flasks. The cells were cultivated by first rinsing the cells twice with phosphate buffered saline (PBS), then trypsinizing for ~2-3 minutes and deactivating the trypsin by adding 2 mL of fresh medium. The cells were removed from the flask surface by gently washing with medium. The solution was then centrifuged at 100 *g* for 5 minutes using an Allegra X-22R Centrifuge (Beckman Coulter). The old medium was removed without disrupting the cell pellets, and then 1 mL of new medium was added to resuspend the cells by gently pipetting up and down. Approximately 20% of the solution containing the cells was then used to further cultivate the cells in 25 cm^2

flasks. Cells were always incubated at 37^{o}C and the CO_2 levels maintained at 5% in a Forma Series II Water Jacketed CO_2 Incubator (Thermo Electron Corporation).

5.2.2: Cell cycle analysis by flow cytometry

Cells were cultured in clear 6-well plates for 24 h in the CO_2 incubator (37^{o}C, 5% CO_2) and treated with 0, 5, 10, 15, 25 and 50 μM CDDP (± 100 μM PM2A) for 12, 24, 48 and 72 h. Both floating and adherent cells were harvested by trypsinization for ~3 minutes and washed twice with PBS by centrifugation (1200 rpm for 8 minutes per cycle). Cells were then fixed and permeabilized using 70% ice-cold ethanol for at least 24 h. Before staining, cells were pelleted and ethanol was removed by aspiration. Then, each sample was washed twice with PBS by centrifugation. Cells were incubated with RNase A (16 μg/mL) for 30 minutes at 37^{o}C and then stained with propidium iodide (50 μg/mL) for 30 minutes in the dark. Samples were analyzed using a BD FACSVantage SE flow cytometer (Becton, Dickinson and Company) in pulse processing mode (10 000 cells/sample) and computational analysis performed using FCS Express software (De Novo Software, Los Angeles, CA) to obtain FL2-A DNA content histograms. Data was gated on front scatter (FSC) versus side scatter (SSC) to eliminate debris, as well as FL2-A versus FL2-W to eliminate doublets. Experiments were performed at least 3 times for each group.

Section 5.3: Results and Discussion

Figures 5.2, 5.4, 5.6, 5.8, 5.10 and 5.12 show cell cycle histograms for cells treated with 0, 5, 10, 15, 25 and 50 μM CDDP only and Figures 5.3, 5.5, 5.7, 5.9, 5.11 and 5.13 for cells treated with 0, 5, 10, 15, 25 and 50 μM CDDP + 100 μM PM2A. Figures 5.14 – 5.19 also indicate the percentages of cells in each cell cycle phase over time for different CDDP concentrations.

Untreated cells exhibited the regular cell cycle distribution as shown in Figure 5.2. This regular cell cycle distribution was also seen for cells treated with only 100 μM PM2A (Figures 5.3 and 5.14). For cells treated with only 5 μM CDDP (Figures 5.4 and 5.15), the distribution was regular at 12 h, but after 24 h, most of the cells accumulated in the S phase. After 48 h, we saw that these cells transitioned past the S-phase and accumulated in the G2/M phase. Most of the cells still arrested in the G2/M phase after 72 h, but some overcame the G2/M checkpoint and transitioned back to the G1 phase. For cells treated with 5 μM CDDP + 100 μM PM2A (Figure 5.5), the distribution was regular at 12 h, but after 24 h, a larger percentage of cells accumulated in the G1 phase as compared to cells treated with only 5 μM CDDP (Figure 5.15). After 48 h, some were still arrested at G1, but some also continued to synthesize DNA in the S-phase and also reached the G2/M phase. After 72 h, the distribution was very similar to that at 48 h, except with a greater percentage of cells in the sub-G1 fraction. Thus, the cells have probably arrested and were not able to transition past their checkpoints.

The cell cycle perturbation pattern for cells treated with 10 μM CDDP only (Figures 5.6 and 5.16) was similar to that of 5 μM CDDP + 100 μM PM2A (Figures 5.5

and 5.15), where the cells arrested earlier in the cell cycle with the addition of PM2A. A 12 and 24 h treatment of 10 μM CDDP + 100 μM PM2A (Figure 5.7) did not perturb the cell cycle distribution. But after 48 h and 72 h, an increase in the percentages of cells accumulating in the early S phase and also in the G1 phase was observed, compared to cells treated with only 10 μM CDDP. An increase in the sub-G1 fraction was also observed (Figure 5.16).

When treated with 15 μM CDDP only (Figures 5.8 and 5.17) for 12 and 24 h, the cells had regular cell cycle distributions. After 48 and 72 h, the cells were relatively spread throughout the cell cycle phases. But with the addition of 100 μM PM2A (Figures 5.9 and 5.17), larger percentages of cells accumulated in the G1 phase instead; this is more evident with the concomitant decrease in the G2 fraction. The distributions for cells treated with 15 μM CDDP for 48 and 72 h were similar to those of 10 μM CDDP + 100 μM PM2A, except the sub-G1 fractions for the cells treated with PM2A were higher.

A large proportion of cells treated with 25 μM CDDP only (Figures 5.10 and 5.18) arrested in the G1 phase, similar to the pattern seen for cells treated with 15 μM CDDP + 100 μM PM2A. Interestingly, the sub-G1 fractions were greater for cells treated with 15 μM CDDP + 100 μM PM2A compared to cells treated with only 25 μM CDDP. The distributions for cells treated with 25 μM CDDP + 100 μM PM2A (Figures 5.11 and 5.18) were similar to those treated without PM2A where most of the cells accumulated in the G1 phase, except the sub-G1 fractions were greater with the addition of PM2A. Similar results were also seen for cells treated with 50 μM CDDP with and without 100 μM PM2A (Figures 5.12, 5.13 and 5.19).

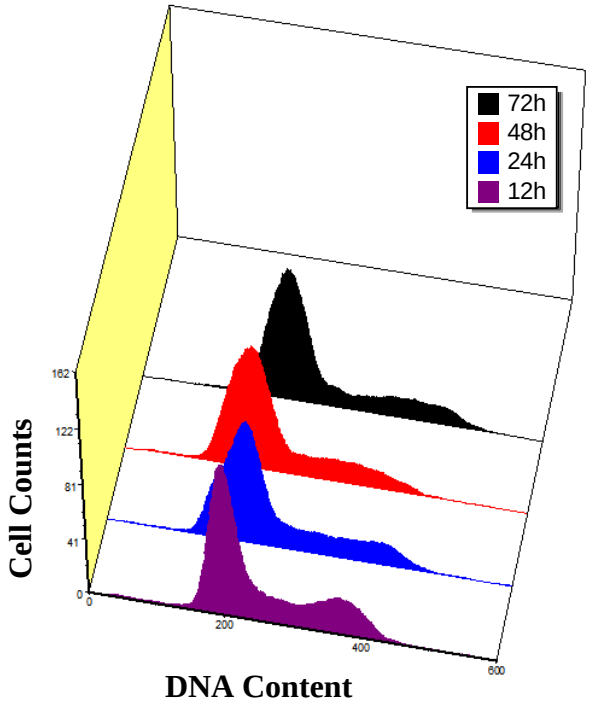

Figure 5.2: Cell cycle distributions for untreated cells (0 μM CDDP) for 12, 24, 48 and 72 h.

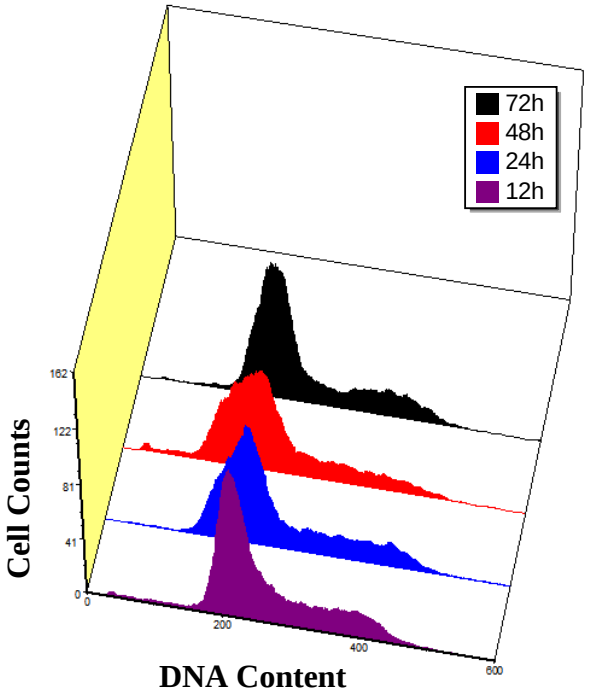

Figure 5.3: Cell cycle distributions for treated cells (0 μM CDDP + 100 μM PM2A) for 12, 24, 48 and 72 h.

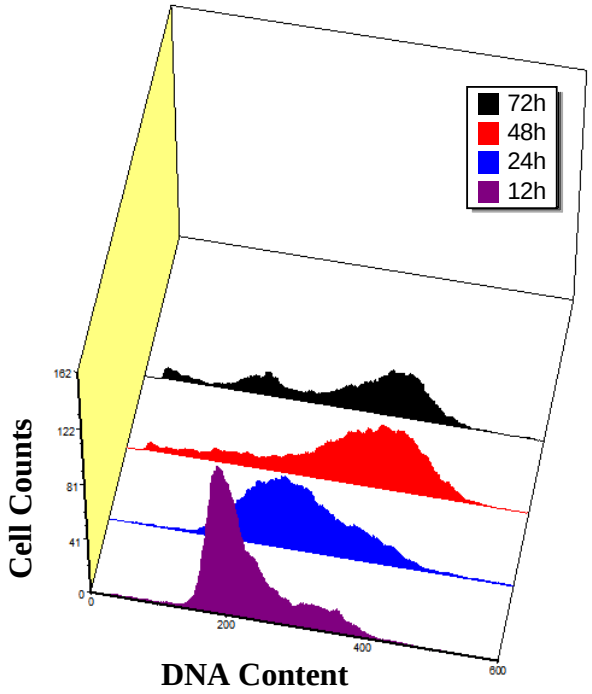

Figure 5.4: Cell cycle distributions for treated cells (5 µM CDDP) for 12, 24, 48 and 72 h.

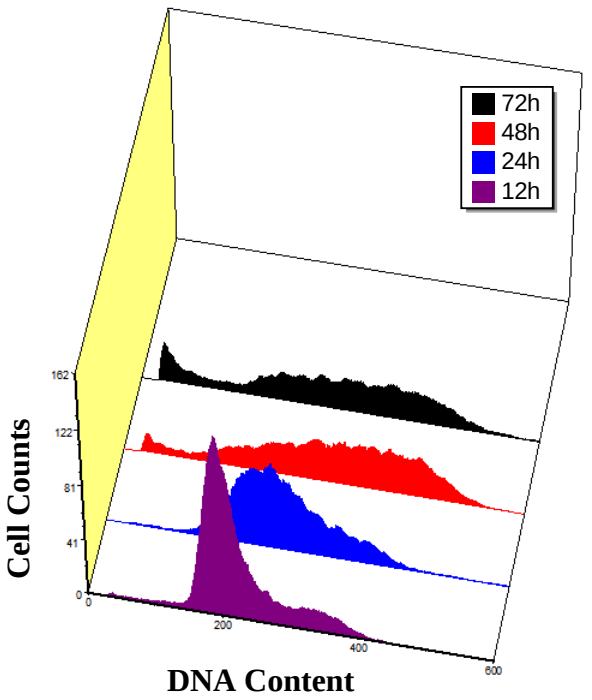

Figure 5.5: Cell cycle distributions for treated cells (5 µM CDDP + 100 µM PM2A) for 12, 24, 48 and 72 h.

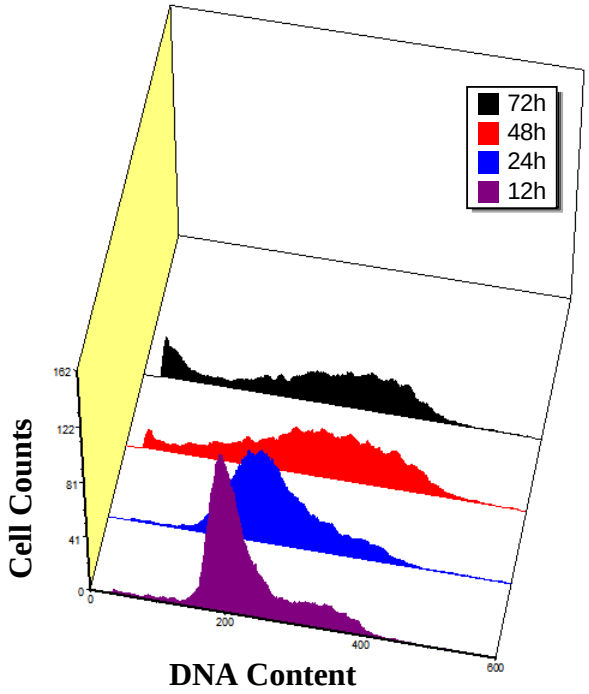

Figure 5.6: Cell cycle distributions for treated cells (10 μM CDDP) for 12, 24, 48 and 72 h.

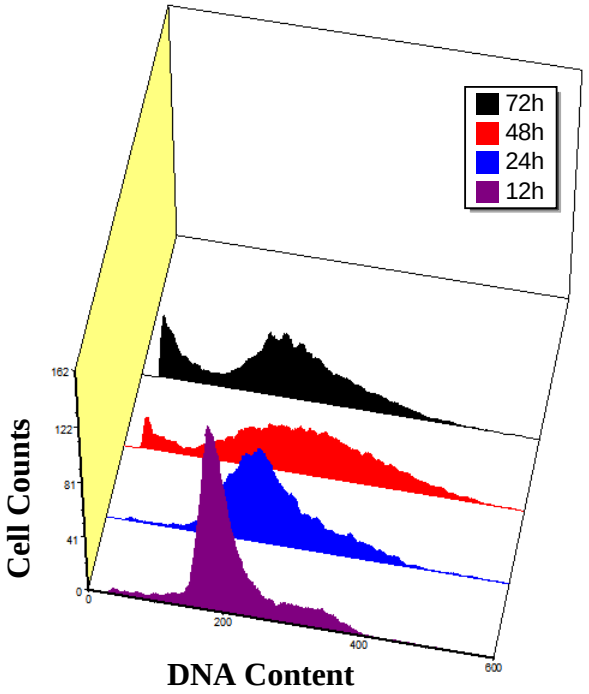

Figure 5.7: Cell cycle distributions for treated cells (10 μM CDDP + 100 μM PM2A) for 12, 24, 48 and 72 h.

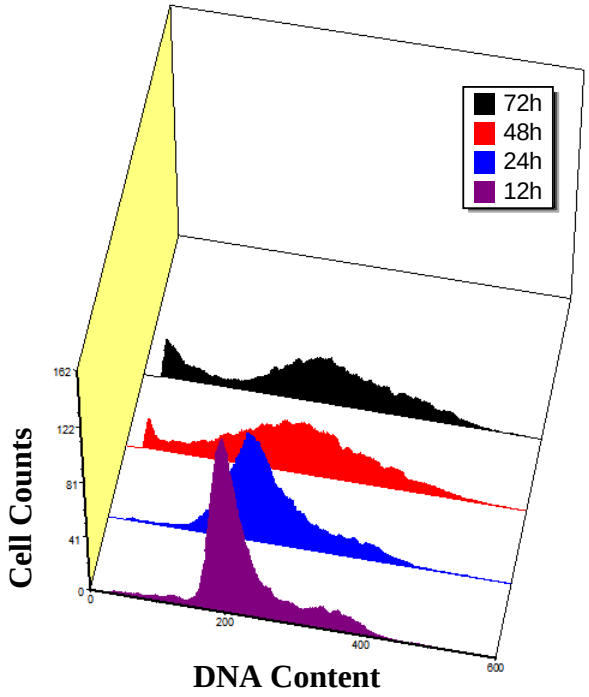

Figure 5.8: Cell cycle distributions for treated cells (15 μM CDDP) for 12, 24, 48 and 72 h.

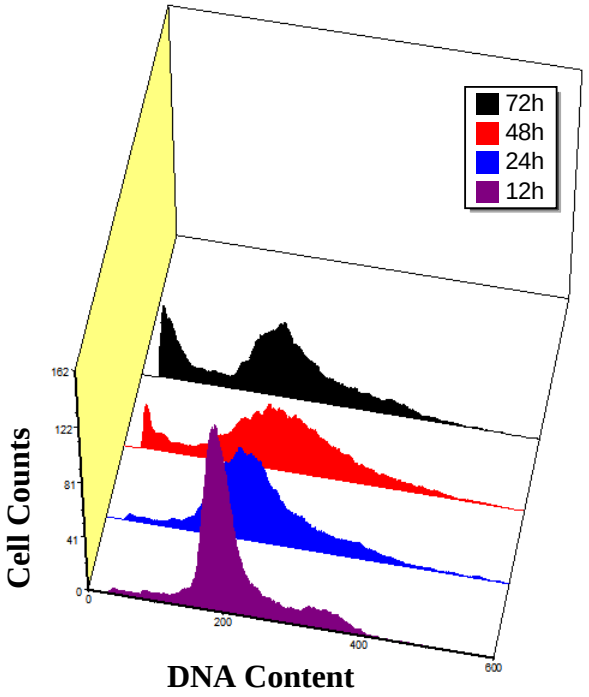

Figure 5.9: Cell cycle distributions for treated cells (15 μM CDDP + 100 μM PM2A) for 12, 24, 48 and 72 h.

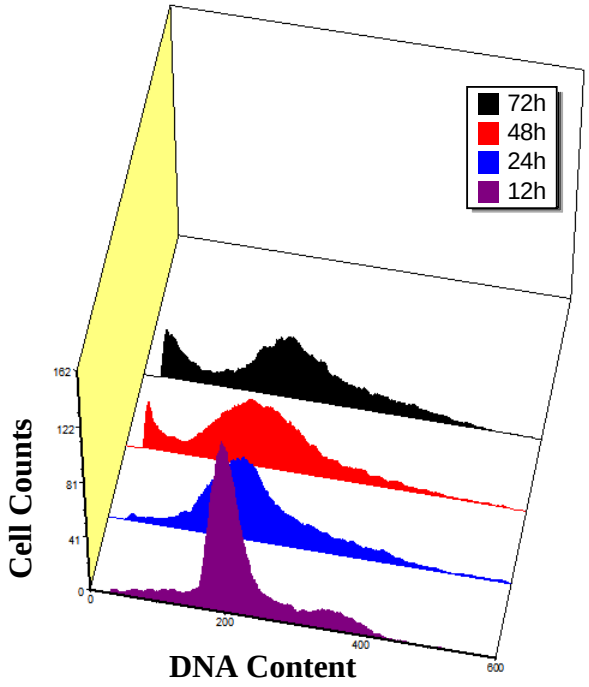

Figure 5.10: Cell cycle distributions for treated cells (25 μM CDDP) for 12, 24, 48 and 72 h.

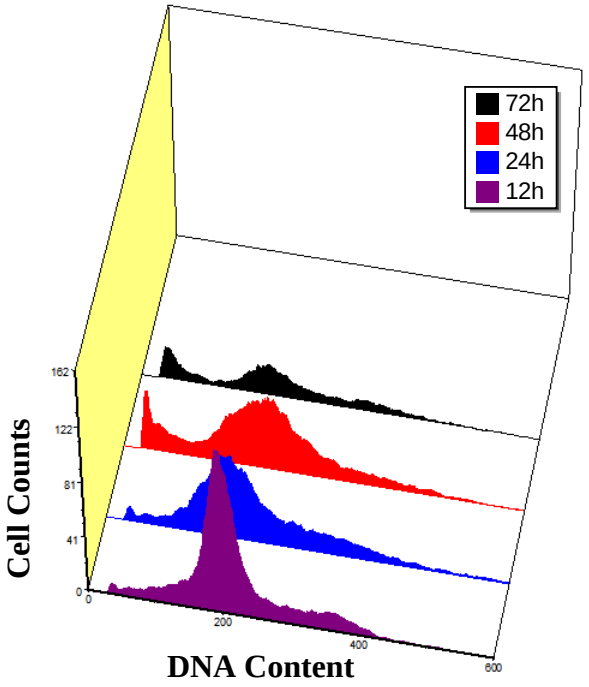

Figure 5.11: Cell cycle distributions for treated cells (25 μM CDDP + 100 μM PM2A) for 12, 24, 48 and 72 h.

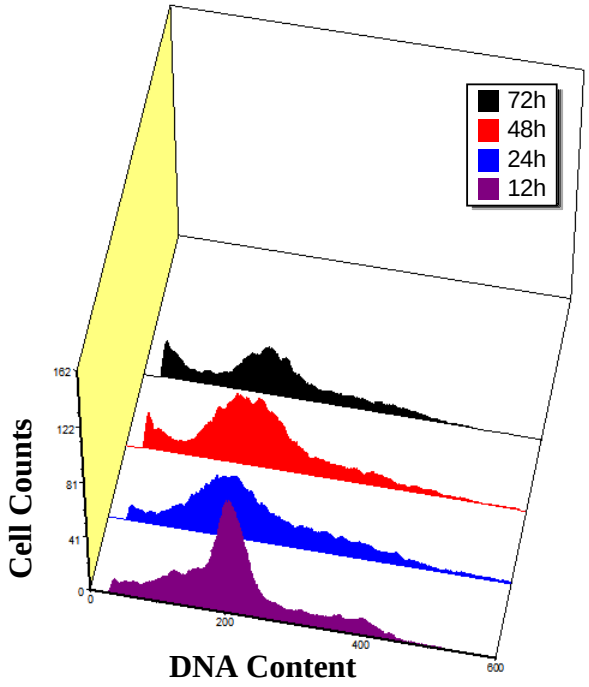

Figure 5.12: Cell cycle distributions for treated cells (50 μM CDDP) for 12, 24, 48 and 72 h.

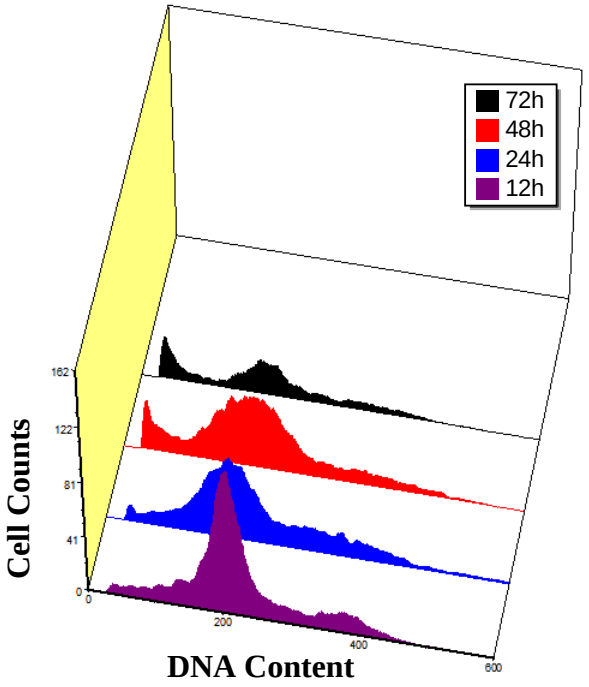

Figure 5.13: Cell cycle distributions for treated cells (50 μM CDDP + 100 μM PM2A) for 12, 24, 48 and 72 h.

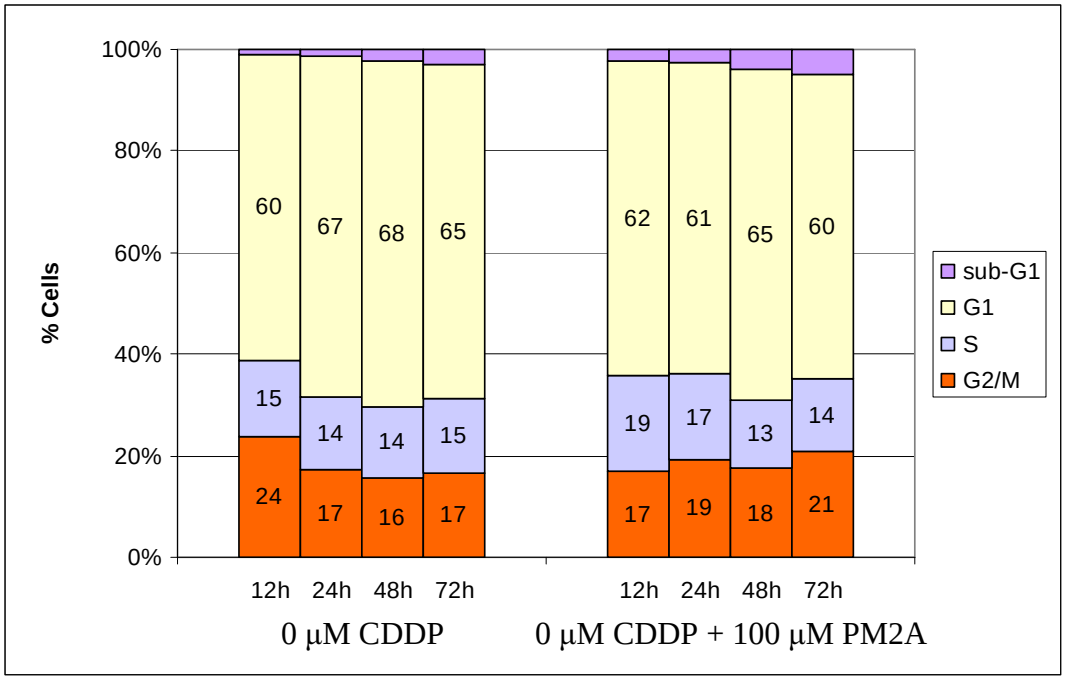

Figure 5.14: Percentages of cells in each phase of the cell cycle for cells treated with 0 µM CDDP (± 100 µM PM2A) at 12, 24, 48 and 72 h.

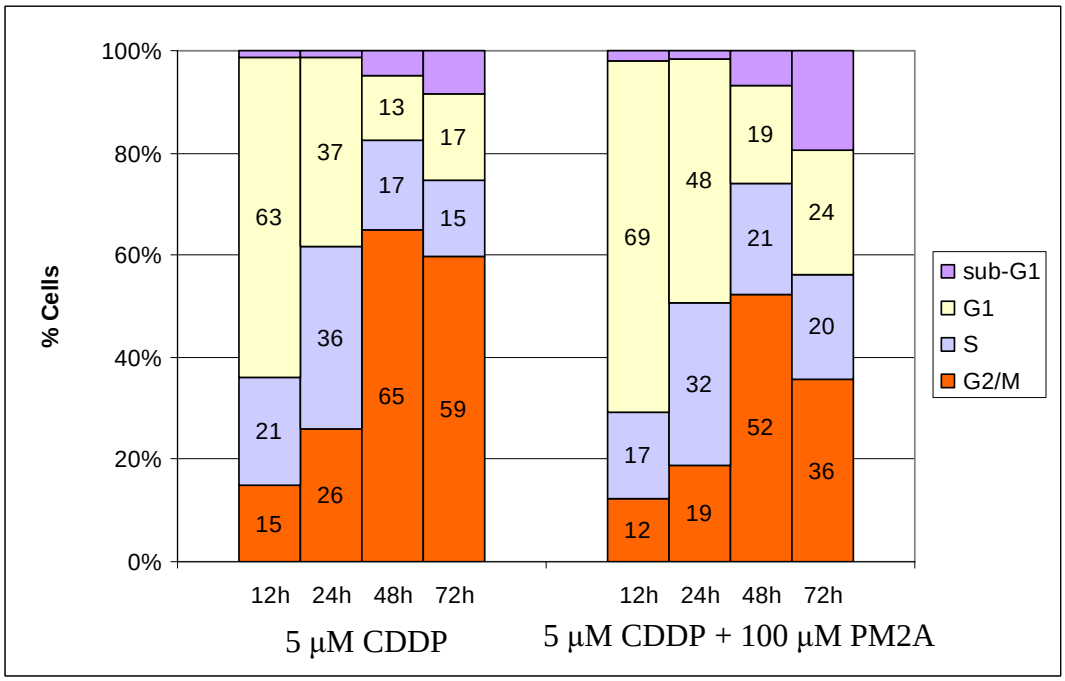

Figure 5.15: Percentages of cells in each phase of the cell cycle for cells treated with 5 µM CDDP (± 100 µM PM2A) at 12, 24, 48 and 72 h.

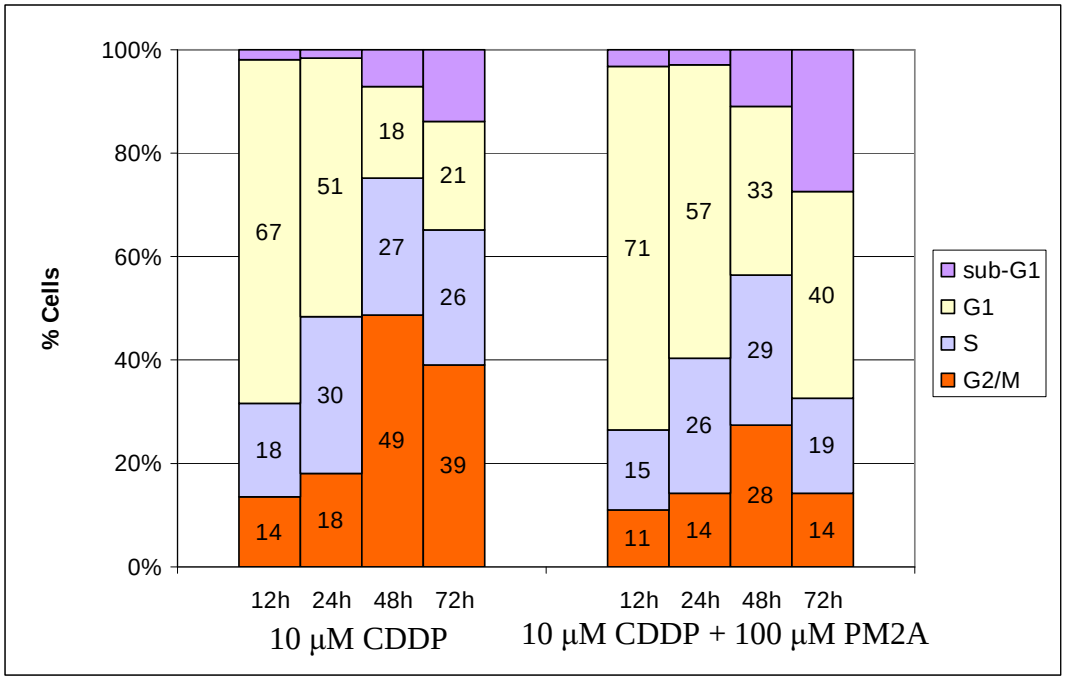

Figure 5.16: Percentages of cells in each phase of the cell cycle for cells treated with 10 µM CDDP (± 100 µM PM2A) at 12, 24, 48 and 72 h.

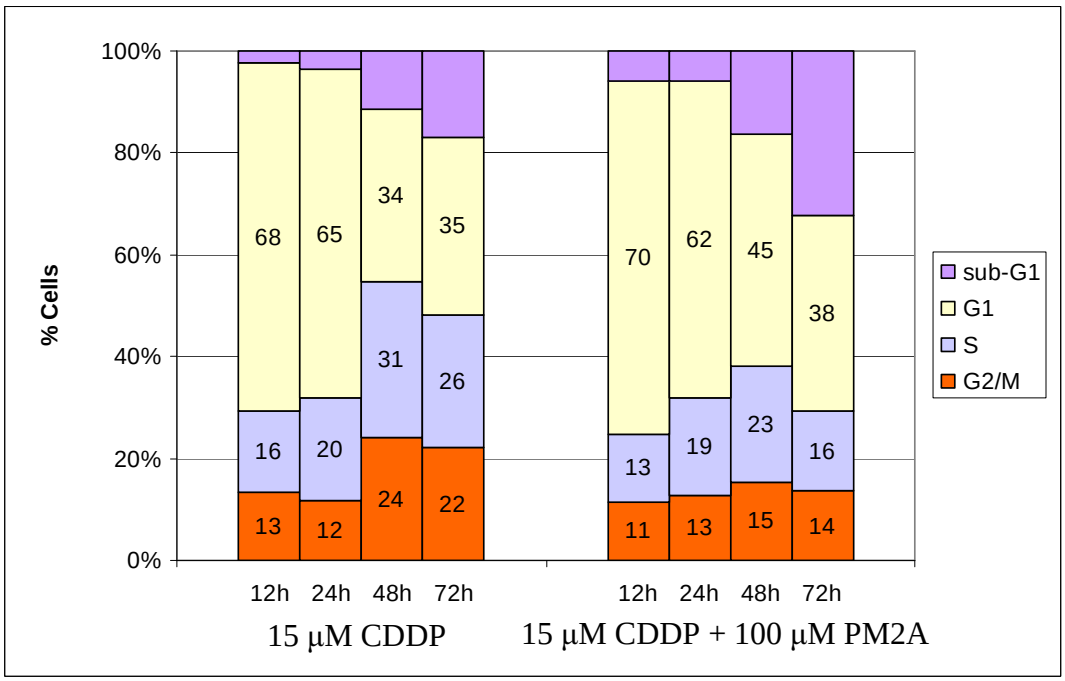

Figure 5.17: Percentages of cells in each phase of the cell cycle for cells treated with 15 µM CDDP (± 100 µM PM2A) at 12, 24, 48 and 72 h.

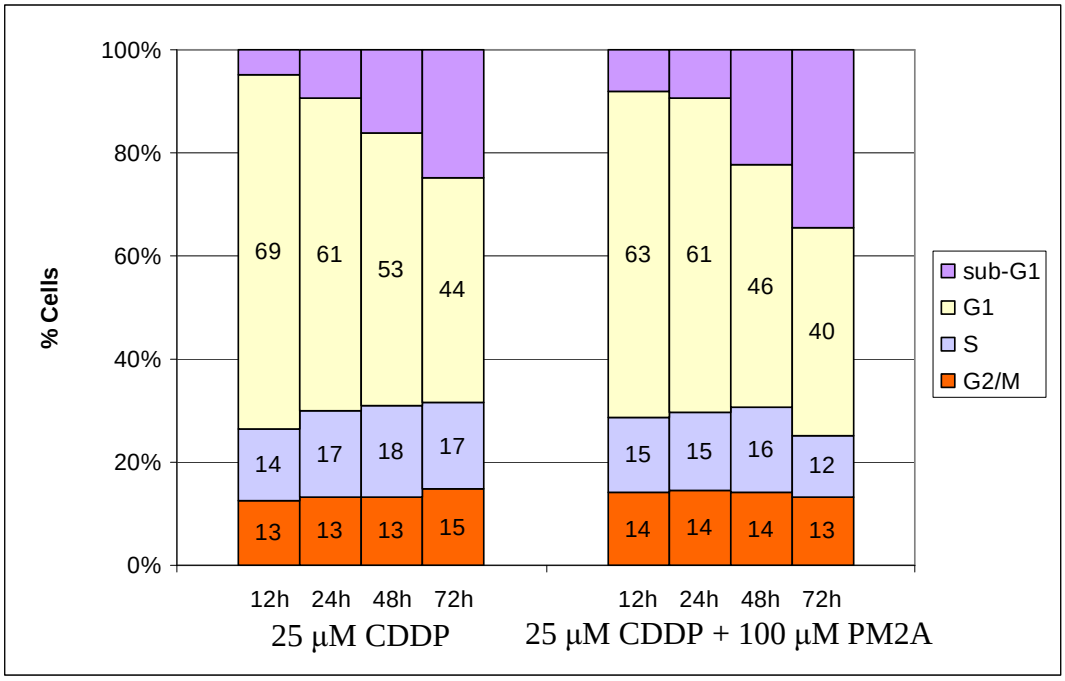

Figure 5.18: Percentages of cells in each phase of the cell cycle for cells treated with 25 µM CDDP (± 100 µM PM2A) at 12, 24, 48 and 72 h.

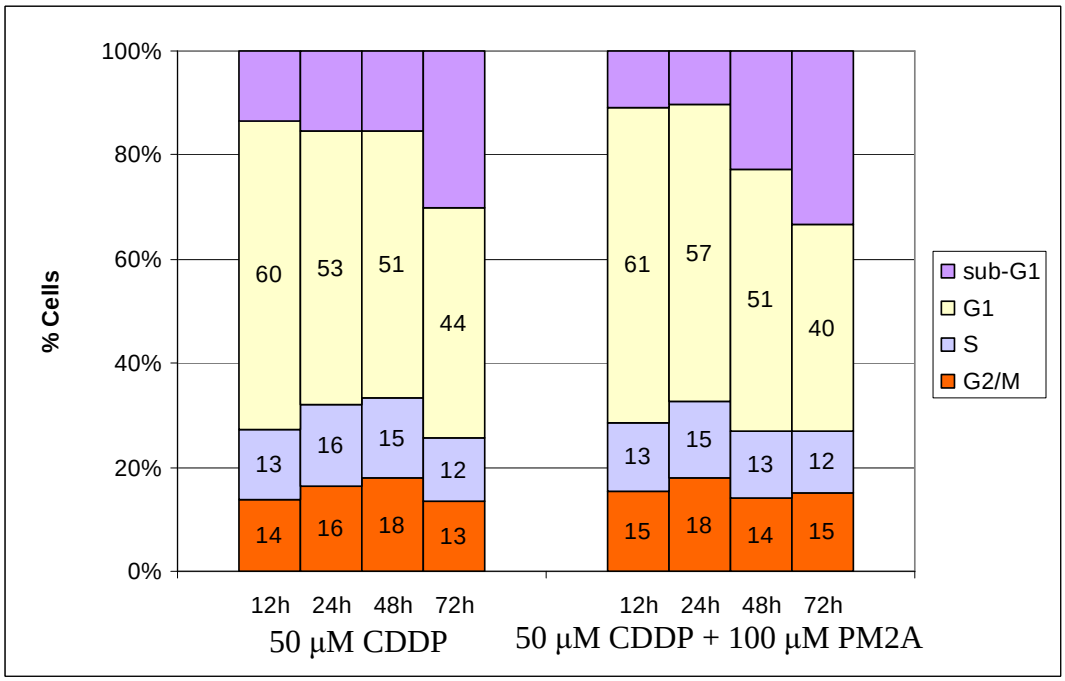

Figure 5.19: Percentages of cells in each phase of the cell cycle for cells treated with 50 µM CDDP (± 100 µM PM2A) at 12, 24, 48 and 72 h.

Section 5.4: Conclusions

By performing cell cycle analysis for different drug concentrations, we were able to observe how the cells transitioned through the cell cycle phases over time. The differences in the cell cycle perturbations were the most obvious for lower concentrations of CDDP. For low concentrations of CDDP, it was found that the cells tended to accumulate in the G2/M phase, although a great proportion of cells were able to transition past their checkpoints to continue dividing. With the addition of PM2A, large percentages of cells were able to accumulate earlier in the cell cycle at the early S phase and even in the G1 phase. Compared to cells treated with only CDDP, those treated with the combination experienced earlier perturbations in the cell cycle. This may allow the cell's machinery to recognize the effects of CDDP more effectively, possibly due to an increased number of CDDP-DNA binding sites and DNA strand breaks. This earlier cell cycle arrest may also suggest that the effects of the combinational regimen are much more severe compared to the effects of the single agents, thus supporting the efficacy of PM2A as a molecular promoter of CDDP.

Chapter 6. DNA Fragmentation by Flow Cytometry

Section 6.1: Introduction

One late stage marker of apoptosis is the degradation of DNA into small fragments. The fragmentation of DNA in apoptotic cells leads to the disintegration of the nucleus, occurring between nucleosomes at ~200-bp intervals [66,67]. An enhancement in the amount of fragmented DNA can give indication to increases in apoptotic events, and thus to the viability of the drug combination.

Detection of DNA fragmentation can be done using the APO-BrdU TUNEL assay, which utilizes the fact that DNA strand breaks expose a large number of 3'-OH ends. The hydroxyl groups act as starting points for terminal deoxynucleotidyl transferase (TdT) to add deoxyribonucleotides. The break sites are labeled by the addition of the deoxythymidine analog 5-bromo-2'-deoxyuridine 5'-triphosphate (BrdUTP) in the presence of the TdT enzyme. An anti-BrdU antibody conjugated with a fluorescent molecule is added to detect the strand breaks by measuring their fluorescence intensities using flow cytometry. The cell cycle distribution can also be detected simultaneously from the ordinate axis of the generated dot plot (with the BrdU-content on the abscissa), where the events with fluorescence intensity above the background indicate the cells with fragmented DNA (within upper box) [76,77]. The dot plots can also indicate the density of the events (number of events per pixel) by the colour, where blue indicates an area with high density of events and red indicates a low density.

Section 6.2: Materials and Methods

6.2.1: Cell culture and treatment

HeLa (cervical cancer cell line) cells were purchased from American Type Culture Collection. The medium for cell culture was minimum essential medium (MEM) with phenol red, which was supplemented with 10% fetal bovine serum (FBS), 100 units/mL penicillin G and 100 μg/mL streptomycin. CDDP (Sigma) was dissolved in ultrapure water and PM2A in pure ethanol, where the final concentration of ethanol was always less than 1% when treated to cells. Ultrapure water with a resistivity of >18.2 MΩ/cm was obtained using a NANOpure DIamond TOC Life Science ultrapure water system (Barnstead International). The cells were split every 3 days, or once they reached a confluency of ~85% in 25 cm^2 flasks. The cells were cultivated by first rinsing the cells twice with phosphate buffered saline (PBS), then trypsinizing for ~2-3 minutes and deactivating the trypsin by adding 2 mL of fresh medium. The cells were removed from the flask surface by gently washing with medium. The solution was then centrifuged at 100 *g* for 5 minutes using an Allegra X-22R Centrifuge (Beckman Coulter). The old medium was removed without disrupting the cell pellets, and then 1 mL of new medium was added to resuspend the cells by gently pipetting up and down. Approximately 20% of the solution containing the cells was then used to further cultivate the cells in 25 cm^2 flasks. Cells were always incubated at 37^oC and the CO_2 levels maintained at 5% in a Forma Series II Water Jacketed CO_2 Incubator (Thermo Electron Corporation).

6.2.2: DNA fragmentation measurement by flow cytometry

Cells were cultured in 25 cm^2 flasks (~8 x 10^7 cells/flask) for 24 h in the CO_2 incubator (37^{o}C, 5% CO_2). The culture medium (~7 mL per flask) was replaced by new medium and incubated for 48 h with varying drug concentrations in the CO_2 incubator. Both floating and adherent cells were harvested by trypsinization for ~3 minutes, washed twice with PBS by centrifugation (300 *g* for 5 min) and fixed using 1% paraformaldehyde for 30 min on ice. Cells were then permeabilized by suspending the cells in 70% ice-cold ethanol for at least 24 h at -20^{o}C. To label the DNA, ethanol was removed after centrifugation and cells were resuspended in 50 μL of TUNEL reaction buffer containing terminal deoxynucleotidyl transferase and BrdUTP for 1 h at 37^{o}C in the dark, shaking every 15 min. After overnight room temperature incubation in the dark, the cells were then incubated with Alexa Fluor 488-conjugated BrdUTP-antibody for 30 min at room temperature in the dark. Cells were also subsequently stained with propidium iodide (5 μg/mL) and incubated with RNase A for 30 min at room temperature to determine the total cellular DNA content. Samples were then analyzed using a Becton-Dickinson FACSVantage SE flow cytometer in pulse processing mode (10 000 cells per sample). Computational analyses were performed using FCS Express software (De Novo Software, Los Angeles, CA) to obtain FL1-H versus FL2-A dot plots (log versus linear, respectively), gating on front scatter (FSC) versus side scatter (SSC) to eliminate debris, as well as FL2-A versus FL2-W to eliminate doublets. Experiments were performed independently at least 3 times.

Section 6.3: Results and Discussion

HeLa cells were treated with 0, 10, 25 and 50 μM CDDP with and without 100 μM PM2A for 48 h. As shown in Figure 6.1, 1% of untreated cells exhibited DNA fragmentation, which can be attributed to cells naturally undergoing cell death. Most of the events were in the G1 phase of the cell cycle, which is characteristic of a regular cell cycle distribution. Figure 6.2 shows that 2% of cells treated with only 100 μM PM2A had DNA fragmentation. When cells were treated with 10 μM CDDP + 100 μM PM2A, the percentages increased from 9% to 18% compared to cells treated with only 10 μM CDDP (Figures 6.3 and 6.4). Remarkably, the percentages increased from 6% to 69% when cells were treated with 25 μM CDDP without and with 100 μM PM2A, respectively (Figures 6.5 and 6.6). The percentages also dramatically increased from 38% to 74% when cells were treated with 50 μM CDDP, without and with 100 μM PM2A, respectively (Figures 6.7 and 6.8). Consistent with the cell cycle analysis in Chapter 5, it was observed that when CDDP was used as a treatment in combination with PM2A, the cells arrested in the early S phase and G1 phase of the cell cycle, whereas the cells tended to accumulate in the G2/M phase for lower doses of CDDP as a single agent. Interestingly, the dot plots indicated that more cells will undergo DNA fragmentation when they are accumulated in the G1 phase. Although cells in all phases of the cell cycle will undergo cell death (non-specific), this will occur maximally for cells in the G1 phase. Thus, there is a significant increase (synergistic) in DNA fragmentation when PM2A is added in combination with CDDP, in correspondence with an earlier arrest of the cells in the S and G1 phases of the cell cycle.

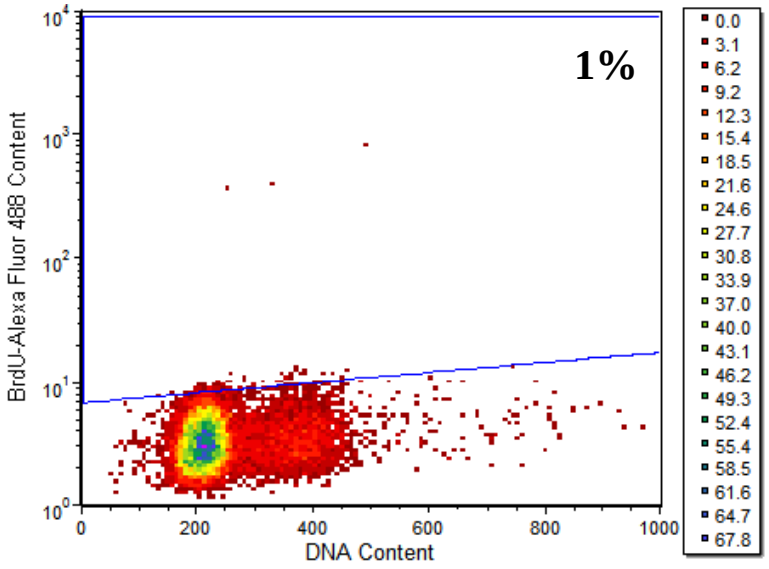

Figure 6.1: Results for APO-BrdU DNA Fragmentation Assay for cells treated with 0 μM CDDP for 48 h. Density plot illustrates BrdU-positive cells as a function of the DNA content (position in the cell cycle). The colours indicate the number of events in each pixel. Three independent trials were performed and the mean percentage of BrdU-positive cells calculated. 1% of cells were BrdU-positive.

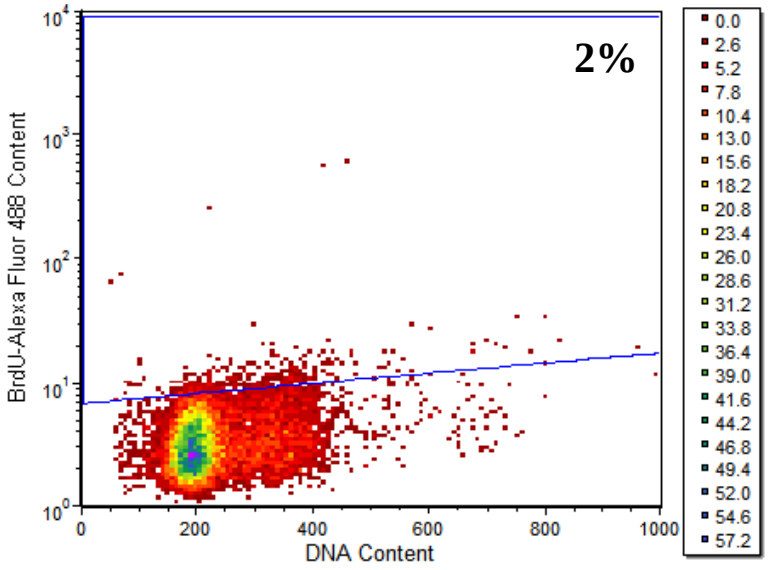

Figure 6.2: Results for APO-BrdU DNA Fragmentation Assay for cells treated with 0 μM CDDP + 100 μM PM2A for 48 h. Density plot illustrates BrdU-positive cells as a function of the DNA content (position in the cell cycle). The colours indicate the number of events in each pixel. Three independent trials were performed and the mean percentage of BrdU-positive cells calculated. 2% of cells were BrdU-positive.

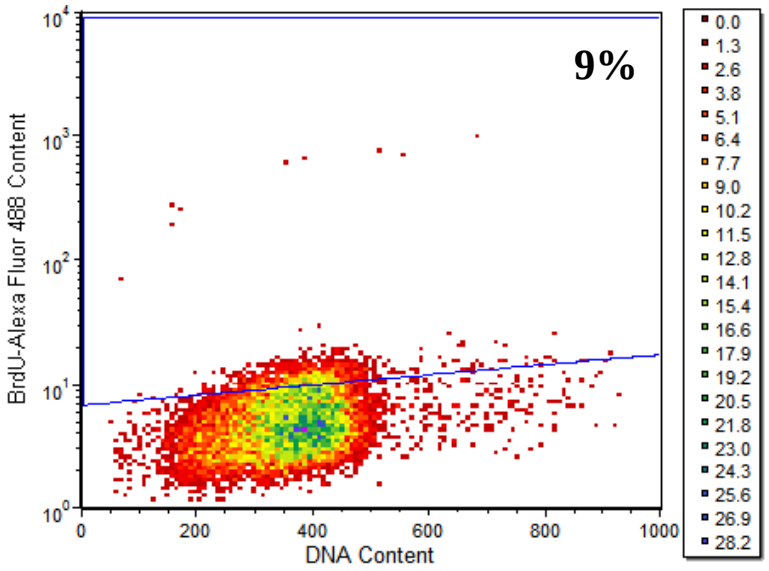

Figure 6.3: Results for APO-BrdU DNA Fragmentation Assay for cells treated with 10 μM CDDP for 48 h. Density plot illustrates BrdU-positive cells as a function of the DNA content (position in the cell cycle). The colours indicate the number of events in each pixel. Three independent trials were performed and the mean percentage of BrdU-positive cells calculated. 9% of cells were BrdU-positive.

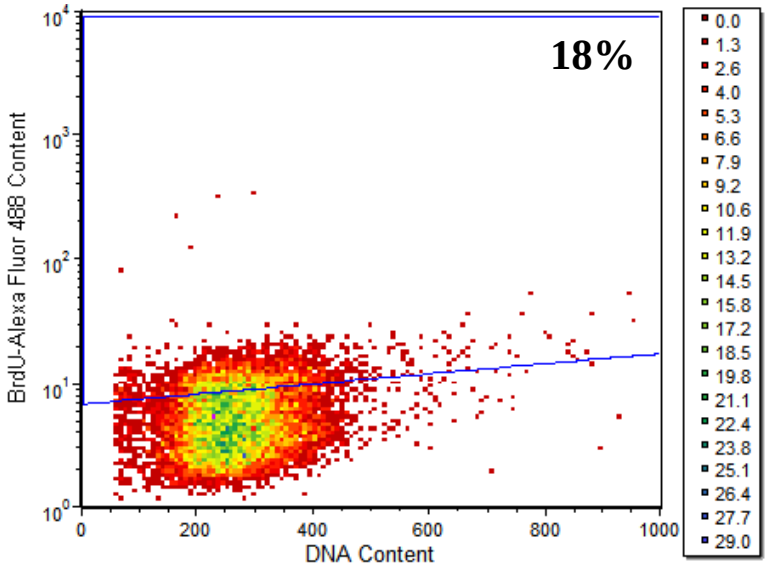

Figure 6.4: Results for APO-BrdU DNA Fragmentation Assay for cells treated with 10 μM CDDP + 100 μM PM2A for 48 h. Density plot illustrates BrdU-positive cells as a function of the DNA content (position in the cell cycle). The colours indicate the number of events in each pixel. Three independent trials were performed and the mean percentage of BrdU-positive cells calculated. 18% of cells were BrdU-positive.

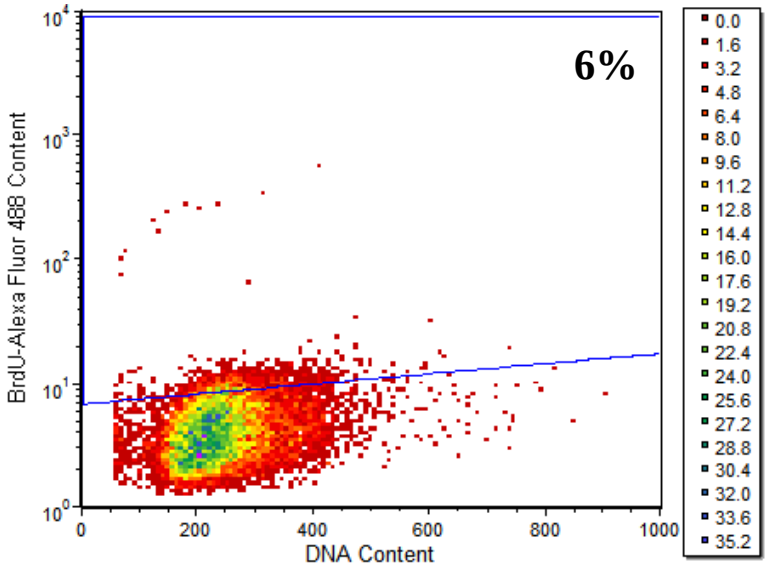

Figure 6.5: Results for APO-BrdU DNA Fragmentation Assay for cells treated with 25 μM CDDP for 48 h. Density plot illustrates BrdU-positive cells as a function of the DNA content (position in the cell cycle). The colours indicate the number of events in each pixel. Three independent trials were performed and the mean percentage of BrdU-positive cells calculated. 6% of cells were BrdU-positive.

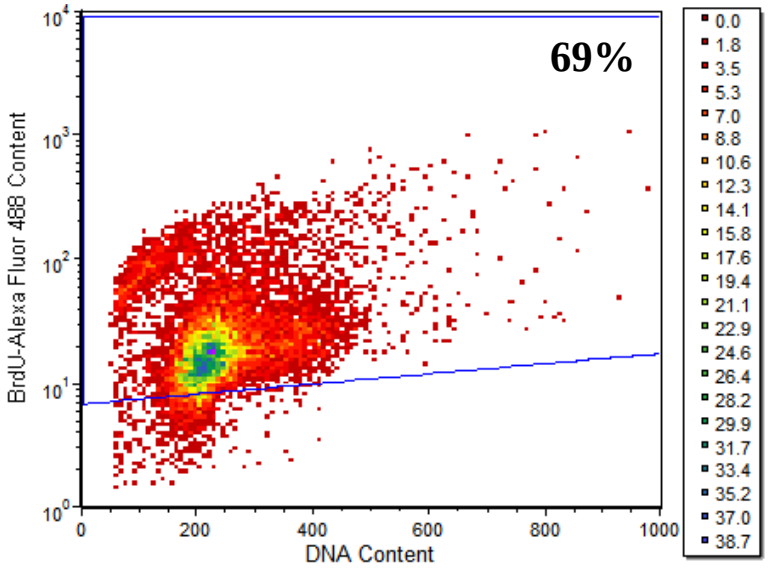

Figure 6.6: Results for APO-BrdU DNA Fragmentation Assay for cells treated with 25 μM CDDP + 100 μM PM2A for 48 h. Density plot illustrates BrdU-positive cells as a function of the DNA content (position in the cell cycle). The colours indicate the number of events in each pixel. Three independent trials were performed and the mean percentage of BrdU-positive cells calculated. 69% of cells were BrdU-positive.

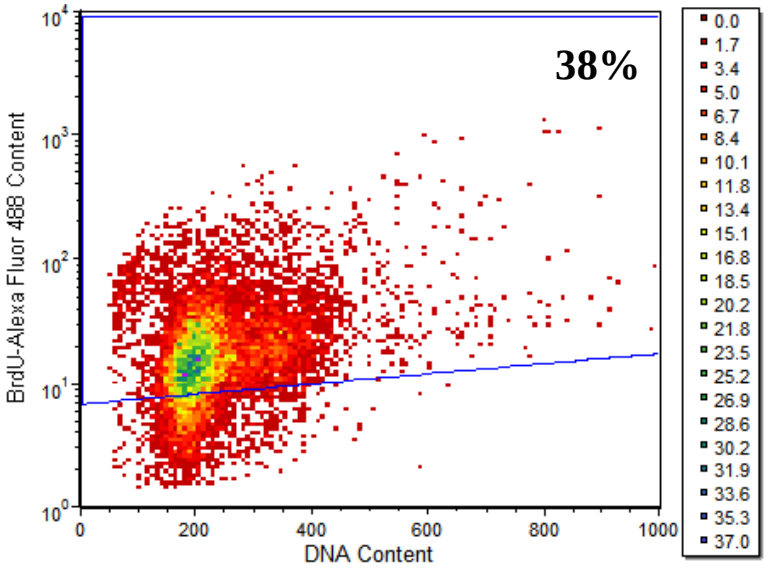

Figure 6.7: Results for APO-BrdU DNA Fragmentation Assay for cells treated with 50 μM CDDP for 48 h. Density plot illustrates BrdU-positive cells as a function of the DNA content (position in the cell cycle). The colours indicate the number of events in each pixel. Three independent trials were performed and the mean percentage of BrdU-positive cells calculated. 38% of cells were BrdU-positive.

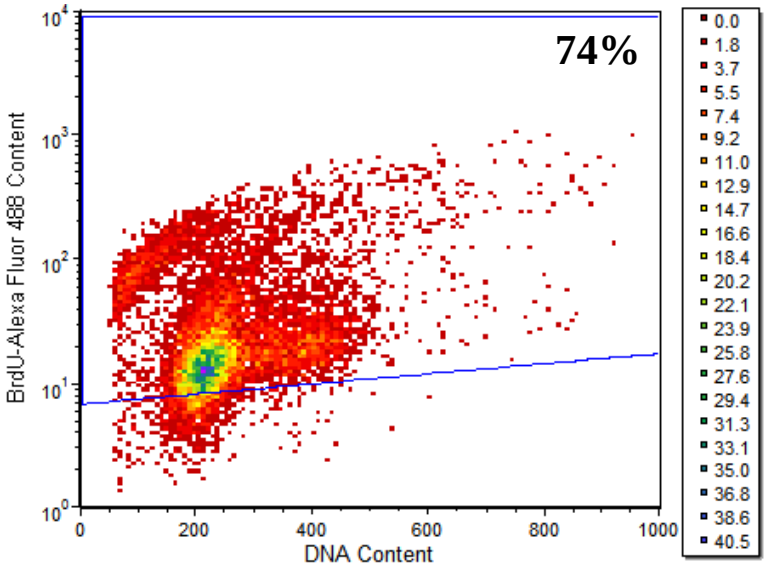

Figure 6.8: Results for APO-BrdU DNA Fragmentation Assay for cells treated with 50 μM CDDP + 100 μM PM2A for 48 h. Density plot illustrates BrdU-positive cells as a function of the DNA content (position in the cell cycle). The colours indicate the number of events in each pixel. Three independent trials were performed and the mean percentage of BrdU-positive cells calculated. 74% of cells were BrdU-positive.

Section 6.4: Conclusions

It is interesting to note that the percentages of DNA fragmentation were relatively the same for cells treated with 10 μM and 25 μM CDDP, although the 10 μM CDDP population mostly arrested at the G2/M phase and the 25 μM CDDP population in the G1 phase. But with the addition of PM2A to CDDP, the increase in DNA fragmentation percentages was significantly greater for 25 μM CDDP than 10 μM CDDP. It is possible that at higher CDDP concentrations (such as 25 μM CDDP) of the drug combination, necrosis is also induced alongside apoptosis. It is also possible that some proportion of cells underwent apoptosis but transitioned to secondary necrosis. This large difference between the high and low concentrations of the combination may also be attributed to the fact that to make the combinational therapy effective, certain concentrations of both CDDP and PM2A must be present inside the cell or more effectively in the cell nucleus. The differences between the high and low concentrations of CDDP can be correlated with the MTT results presented in Chapter 3. A relatively small increase in the cell survival rates were seen when PM2A was added to CDDP concentrations less than 20 μM, whereas significantly large differences were seen for CDDP concentrations greater than 20 μM.

Although PM2A, as a single agent, had minimal effects on DNA fragmentation of HeLa cells, it was shown that the addition of this compound to CDDP greatly enhanced its DNA fragmentation effects. Furthermore, this synergistic enhancement also corresponded to earlier cell cycle arrests in the S and G1 phases, as compared to G2/M

arrest for cells treated with only CDDP. This provides evidence as to why and how PM2A is able to enhance the efficacy of CDDP on a cellular level.

Chapter 7. Absorption Spectroscopic Analysis

Section 7.1: Introduction

Solvents providing reductive environments such as ethanol may be able to prevent PM2A from losing its electron. On the other hand, the tendency for PM2A to donate its electron is highly probable in oxidative environments such as water with the presence of oxygen; thus, PM2A is expected to be quite unstable in aerobic water environments. Furthermore, the presence of an electron-accepting molecule (relative to PM2A) would result in the competition of the electron between this constituent and oxygen. We expect to observe this competition of the electron from PM2A between CDDP and oxygen.

The static absorbance spectra of PM2A under several conditions were obtained to determine its reactivity in different solvent environments over time since absorbance spectroscopy probes electronic transitions.

Section 7.2: Materials and Methods

Static UV/Vis absorption spectroscopy was performed for a 100 μM PM2A solution in pure ethanol, 100 μM PM2A solution in 1% ethanol and 100 μM PM2A + 50 μM CDDP solution in 1% ethanol. 10 mM PM2A stock solutions were prepared in pure ethanol immediately before measurements. Cisplatin (Sigma) was dissolved in ultrapure water. Ultrapure water with a resistivity of >18.2 MΩ/cm was obtained using a NANOpure

DIamond TOC Life Science ultrapure water system (Barnstead International). Absorbance readings were scanned from 190 nm to 1000 nm at different time points after the initiation of the reaction (through mixing of the solution by inversion) using a DU 530 Life Science UV/Vis Spectrophotometer (Beckman Coulter). Absorbance measurements were made in quartz cuvettes and all experimental steps (including sample preparation) were performed in the dark. The baseline for measurements were made with pure ethanol for the 100 μM PM2A solution in pure ethanol sample, and made in ultrapure water for the 100 μM PM2A solution in 1% ethanol and 100 μM PM2A + 50 μM CDDP solution in 1% ethanol samples.

Section 7.3: Results and Discussion

Figure 7.1 shows the absorbance spectrum of 100 μM PM2A in pure ethanol. The spectrum was measured at various time points between 0 to 24 h, but it was found that it did not change during this time period. Absorbance peaks were observed at 204 nm, 261 nm and 314 nm.

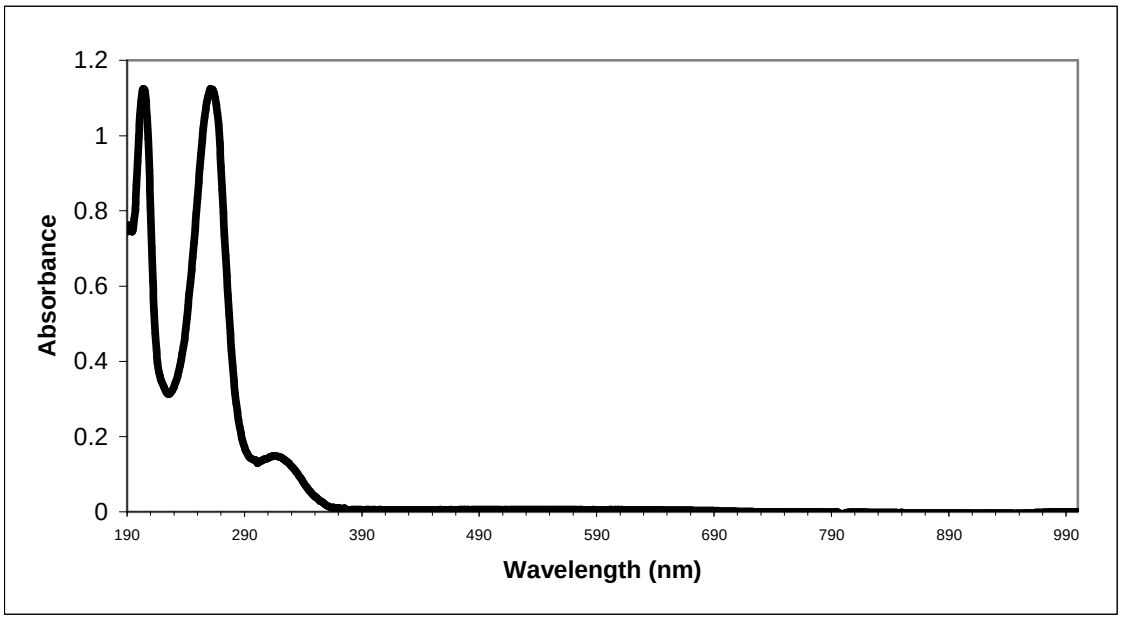

Figure 7.1: Static absorption spectrum for 100 μM PM2A in pure ethanol. The spectrum did not change over the 24 h period.

In *in vitro* experiments, the percentage of the PM2A vehicle was always 1% ethanol. As evident from Figures 7.1 and 7.2, the absorbance spectrum for 100 μM PM2A in 1% ethanol at the beginning of the reaction (0 h) was slightly different from that in pure ethanol. Peaks were seen at 196 nm, 255 nm, 325 nm, 561 nm and 612 nm. The peaks at 196 nm, 255 nm and 325 nm corresponded to peaks at 204 nm, 261 nm and 314 nm in the 100 μM PM2A in pure ethanol spectrum, but slightly shifted.

Absorbance spectra were measured for 100 μM PM2A in 1% ethanol for varying points and were found to change over time. The spectra at 0, 2 and 8 h are shown in Figure 7.2. Initially, peaks were seen at only 196 nm and 255 nm. Additional peaks at 325 nm, 561 nm and 612 nm started to form shortly after the start of the reaction. The additional peaks at 561 nm and 612 nm were not seen in the 100 μM PM2A in pure ethanol spectrum. The isobestic point occurred at 283 nm; thus, the absorbances at wavelengths less than 283 nm decreased over time, and those at wavelengths greater than 283 nm increased over time.

The spectra were also measured for 100 μM PM2A in 1% ethanol with the addition of 50 μM CDDP, as shown in Figure 7.3. CDDP only had some absorbance at 196 nm but did not have absorbance at wavelengths greater than this. At the beginning of the measurement (0 h), the spectrum for 100 μM PM2A + 50 μM CDDP in 1% ethanol was very similar to that of only 100 μM PM2A in 1% ethanol, having the same peak positions. Measurements are shown for 0, 2 and 8 h after the initiation of the reaction. The spectra also changed over time, having the same isobestic point at 283 nm.

Since the absorbance spectra changed over time for 100 μM PM2A (± 50 μM CDDP) in 1% ethanol, the absorbance values were plotted as a function of time for each

peak wavelength (refer to Figures 7.4-7.8). For all peak wavelengths, the absolute rates of change for the absorbances were greater with the addition of CDDP. For peak wavelengths 196 nm and 255 nm (wavelengths less than the isobestic point), the absorbance values decreased at greater rates for 100 μM PM2A + 50 μM CDDP (Figures 7.4 and 7.5). On the other hand, the absorbance values increased at greater rates for 100 μM PM2A + 50 μM CDDP (Figures 7.6, 7.7 and 7.8) for peak wavelengths 325 nm, 561 nm and 612 nm (wavelengths greater than the isobestic point).

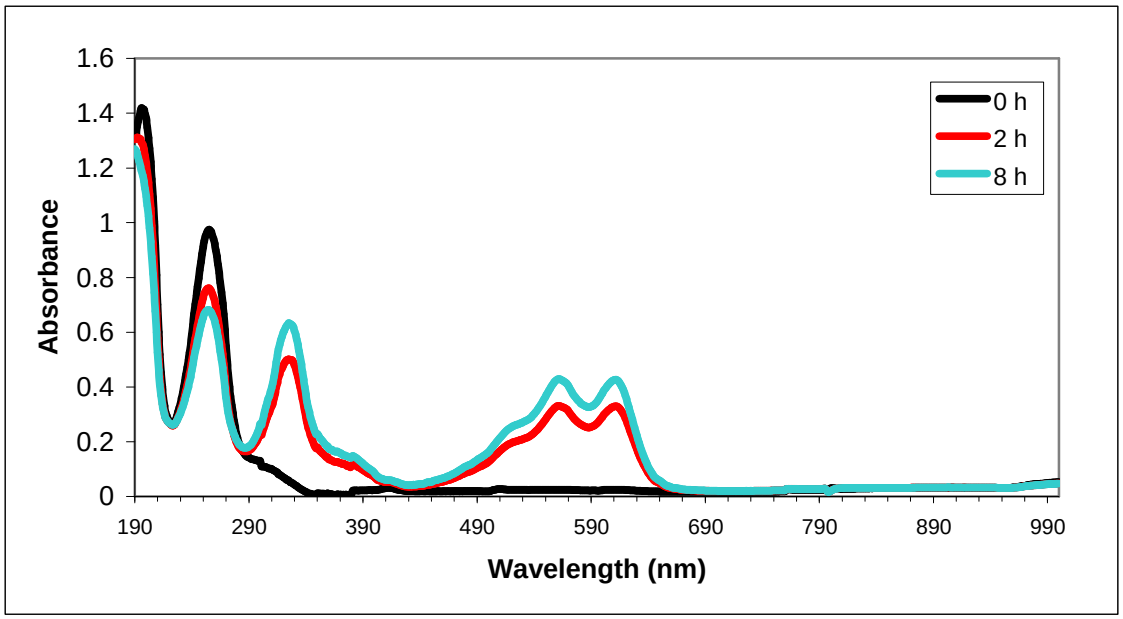

Figure 7.2: Static absorption spectrum for 100 μM PM2A in 1% ethanol at 0, 2 and 8 h time points.

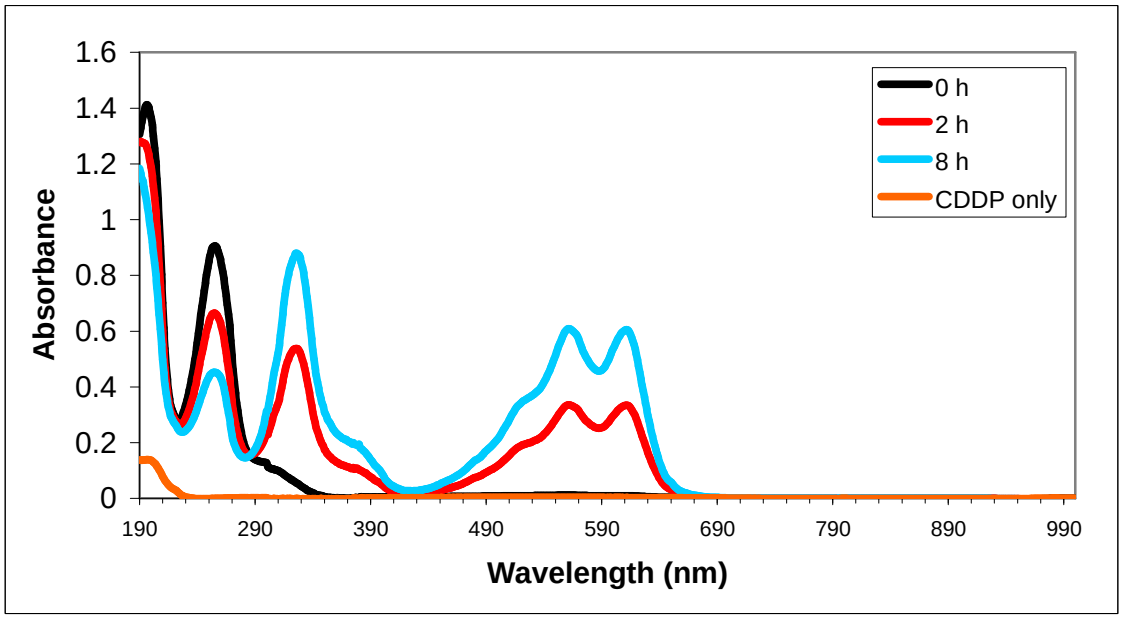

Figure 7.3: Static absorption spectrum for 50 μM CDDP + 100 μM PM2A in 1% ethanol at 0, 2 and 8 h time points. The spectrum for only 50 μM CDDP is also shown.

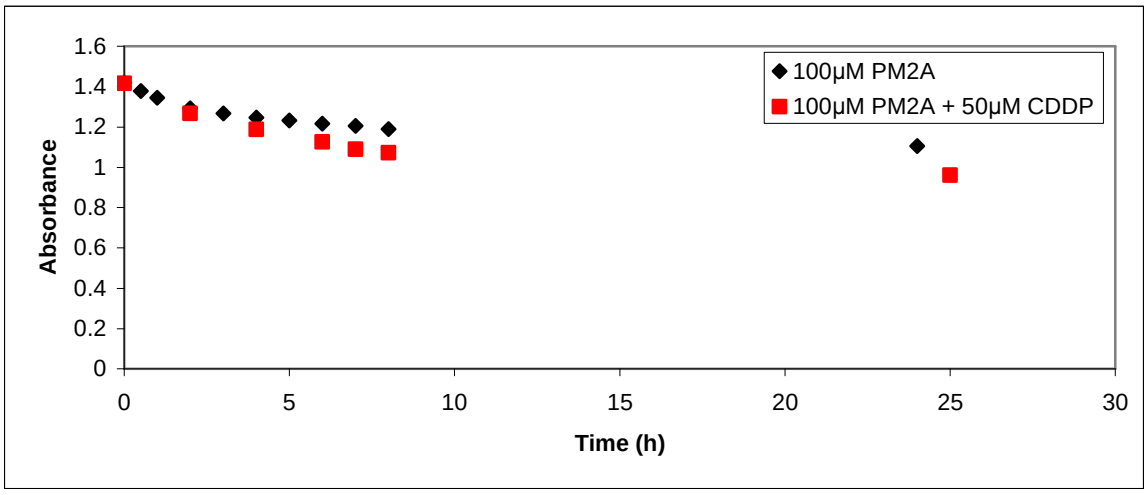

Figure 7.4: The change in the absorbance spectra over time at the 196 nm peak for 100 μM PM2A and 50 μM CDDP + 100 μM PM2A, both in 1% ethanol.

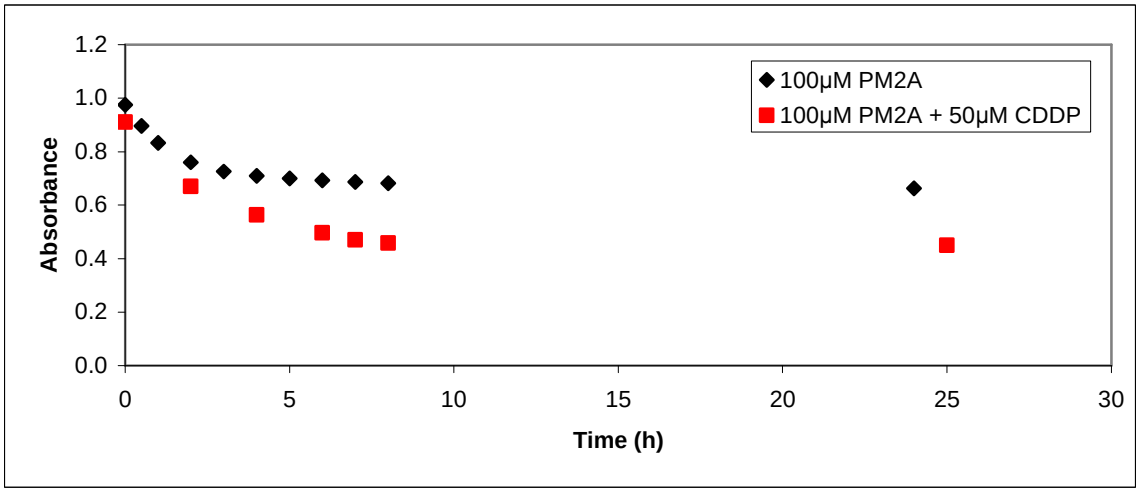

Figure 7.5: The change in the absorbance spectra over time at the 255 nm peak for 100 μM PM2A and 50 μM CDDP + 100 μM PM2A, both in 1% ethanol.

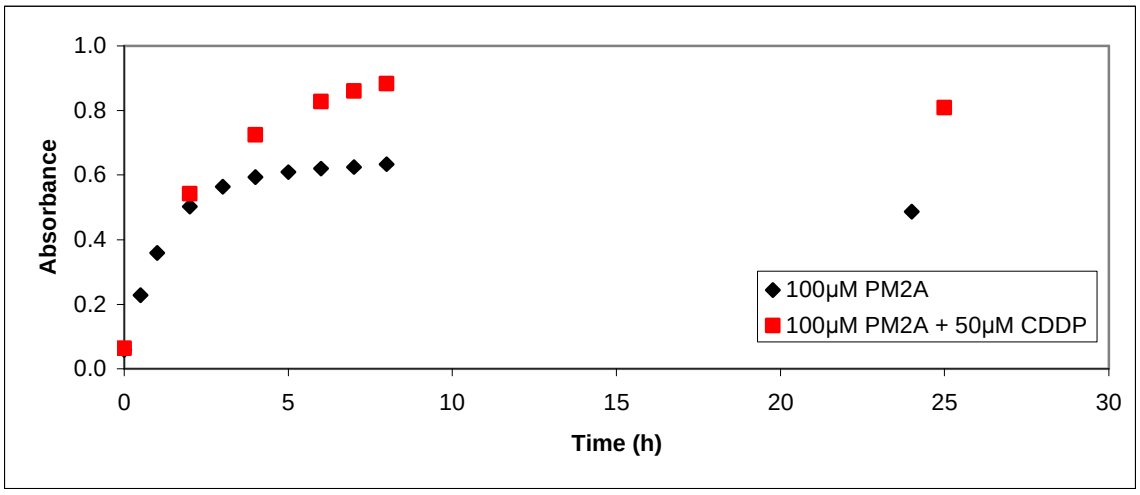

Figure 7.6: The change in the absorbance spectra over time at the 325 nm peak for 100 μM PM2A and 50 μM CDDP + 100 μM PM2A, both in 1% ethanol.

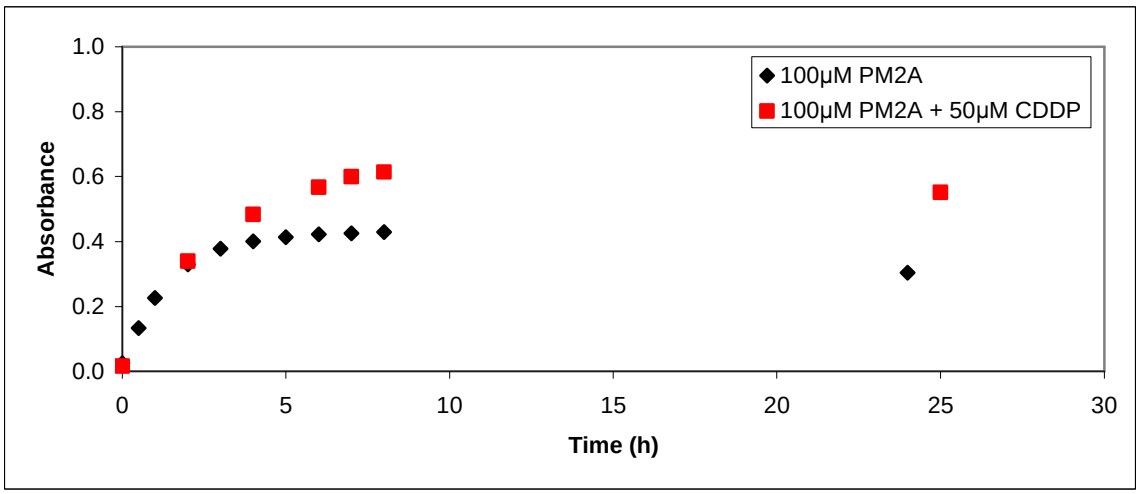

Figure 7.7: The change in the absorbance spectra over time at the 561 nm peak for 100 μM PM2A and 50 μM CDDP + 100 μM PM2A, both in 1% ethanol.

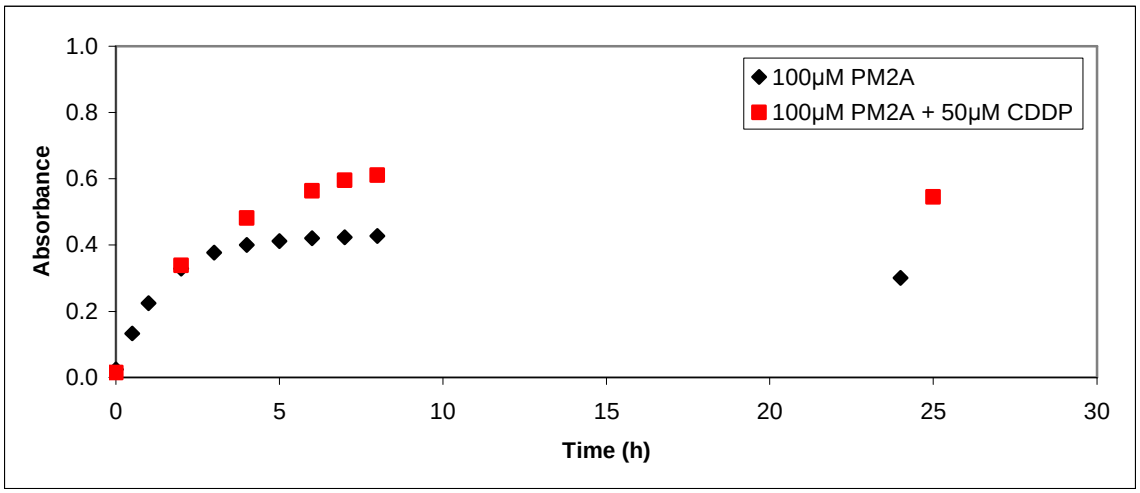

Figure 7.8: The change in the absorbance spectra over time at the 612 nm peak for 100 μM PM2A and 50 μM CDDP + 100 μM PM2A, both in 1% ethanol.

Section 7.4: Conclusions

It was observed that the absorbance spectra for PM2A dissolved in pure ethanol did not change over time; thus showing its stability in a reductive environment. The changes in the absorbance spectra of 100 μM PM2A in 1% ethanol over time most likely indicated the instability of PM2A in an oxidative environment. On the other hand, the changes in the absorbance spectra of 100 μM PM2A in 1% ethanol increased with the addition of CDDP. This indicates the electron-transfer reaction between PM2A and CDDP.

Chapter 8. Conclusions

In this study, it was shown that one should *not* simply follow the classical criterion for designing combinational chemotherapeutic drug regimens. To reiterate from Section 1.3, the criteria are the following [1,2,3]:

- Each drug should be active when used alone
- Drugs should have different mechanisms of antitumor action
- The toxic side effects of the drugs should not overlap so that each drug can be given at or near their maximum tolerated dose
- Drugs should have different resistance profiles
- Drugs may target different cell cycle phases

Ideally, if one were to design a drug regimen where one drug can synergistically potentiate the action of another, additional toxic side effects should not be introduced into the specimen. The introduction of additional toxic side effects to a wider range of organs is a direct consequence of the classical criterion. In order to limit the drug toxicities, it is recommended that each drug should not be active when used alone, they should not have different mechanisms of antitumor action, their toxic side effects should overlap and they may not need to have different resistance profiles or target different cell cycle phases.

The results of this study are direct evidence that a new criterion is urgently needed and that the classic criterion should not mechanically followed. The viability of the molecular promoter PM2A in enhancing the cytotoxic effects of CDDP in a cervical cancer cell line was shown, while introducing minimal additional toxicities. PM2A was chosen as the molecular promoter based on the new mechanistic understanding of how

CDDP is able to attack DNA [32,33]. It is now understood that the cytotoxic action of CDDP can be attributed to its high reactivity with weakly-bound precursor electrons, thus being able to preferentially bind to guanine bases and generating DNA-damaging radicals. The role of PM2A is to enhance the DNA-damaging effects of CDDP by donating its electrons to CDDP to generate more radicals. Thus, the administered doses of CDDP may be reduced, while still producing the same or even higher therapeutic effects. By reducing the doses of CDDP, its toxic side effects are also halted.

First, the MTT assay was used to evaluate the effects of the drug combination on cell survival rates. Then, fluorescence microscopy was used to visualize the differences in the cell morphological changes between the single agents and the combination regimen; in particular, it was hoped to observe increases in the number of apoptotic cells in the combinational regimen. These methods showed significant increases in the number of dead cells when the cancer cells were treated with both PM2A and CDDP.

Flow cytometry was then used to perform cell cycle analysis, in which cell cycle perturbations were observed. While a treatment of low doses of CDDP caused arrest in the G2/M phase of the cell cycle, the combination of PM2A + CDDP resulted in accumulations earlier in the cell cycle (S phase and even the G1 phase). This also resulted in increases in the sub-G1 fraction.

Flow cytometry was also used to analyze the amount of cells exhibiting increased percentages of DNA fragmentation, a landmark of apoptosis. The addition of PM2A to CDDP treatment to HeLa cells significantly increased the levels of DNA fragmentation. Furthermore, this also corresponded to earlier cell cycle arrest in the G1 phase, giving possible implications as to how the cell undergoes apoptosis on a cellular level.

Furthermore, the synergistic action of the drug combination should only be localized to the tumor site. By taking advantage of the hypoxic environment of tumors, the cell-killing effects of CDDP may be enhanced only at tumor sites. In other words, PM2A would only be able to lose its electron to CDDP, thus enhance its effects, at the tumor site (in hypoxic or reductive environments). On the contrary, PM2A should be oxidized by the aerobic environment (oxygen present in water, for example) and be limited in donating its electron to CDDP. These criteria are very important in localizing the antitumor action and limiting the toxic side effects. This localizability is based on the electron-transfer mechanism between PM2A and CDDP. Absorption spectroscopic studies showed that the absorption spectra of PM2A are drastically changed by the presence of CDDP. This suggests the strong electron-transfer reaction between PM2A and CDDP, consistent with the finding that CDDP is a very effective electron acceptor and the fact that PM2A is a well-known biological electron donor. The spectra of PM2A were very stable over time in a reductive environment, suggesting that it would be able to preferentially react with CDDP in hypoxic environments. The spectra of PM2A were unstable over time in an oxidative environment, indicating that a limited amount of PM2A would be able to donate its electrons to CDDP, thus greatly reducing the cytotoxic action at non-hypoxic sites (non-tumor sites, for example).

In closing, this work implicates that clinical doses of CDDP can be significantly reduced when administered in combination with PM2A, thus minimizing the toxic side effects that CDDP-treated patients currently experience, since PM2A alone exhibits minimal detrimental effects. Effectively, this would greatly decrease the number of

patients who suffer from toxic-related deaths and thus, significantly improve the prognosis of cancer patients.

References

[1] Garth, P. and Miles, H. *The toxicity of anticancer drugs* (Pergamon Press, New York, 1991).

[2] Dorr, R. and Von Hoff, D. *Cancer chemotherapy handbook* (Appleton & Lange, Connecticut, 1994).

[3] Perry, M. *The chemotherapy source book* (Wolters Kluwer Health, Philadelphia, 2008).

[4] "Cancer Treatment." National Cancer Institute. April 1 2010, <www.cancer.gov>.

[5] Hussain, S. and James, N. The systemic treatment of advanced and metastatic bladder cancer. Lancet Oncology **8**, 489-497 (2003).

[6] Rosenberg, B., van Camp, L. and Krigas, T. Inhibition of cell division in *Escherichia coli* by electrolysis products from a platinum electrode. Nature **205**, 698-699 (1965).

[7] Minotti, G. et al. Anthracyclines: Molecular Advances and Pharmacologic Developments in Antitumor Activity and Cardiotoxicity. Pharmacological Reviews **56**, 185-229 (2004).

[8] Williams, K. et al. Bioreductive drugs: from concept to clinic. Clinical Oncology **19**, 427-442 (2007).

[9] Jaffar, M. et al. Bioreductive and gene therapy approaches to hypoxic diseases. Adv Drug Deliv Rev **53**, 217-228 (2001).

[10] Kennedy, K. et al. The hypoxic tumor cell: a target for selective cancer chemotherapy. Biochem Pharmol **29**, 1-8 (1980).

[11] Zeman, E. et al. SR-4233: a new bioreductive agent with high selective toxicity for hypoxic mammalian cells. Int J Radiat Oncol Biol Phys **12**, 1239-1242 (1986).

[12] Siim, B. et al. Tirapazamine-induced cytotoxicity and DNA damage in transplanted tumors: relationship to tumor hypoxia. Cancer Research **57**, 2922-2928 (1997).

[13] Patterson, A. et al. Importance of P450 reductase activity in determining sensitivity of breast tumor cells to the bioreductive drug, tirapazamine (SR 4233). Br J Cancer **72**, 1144-1150 (1995).

[14] Garner, A. et al. Nitric oxide synthases catalyze the activation of redox cycling and bioreductive anticancer agents. Cancer Research **59**, 1929-1934 (1999).

[15] Denny, W. The design of drugs that target tumour hypoxia. Aust J Chem **57**, 821-828 (2004).

[16] Koch, C. Unusual oxygen concentration dependence of toxicity of SR-4233, a hypoxic cell toxin. Cancer Research **53**, 3992-3997 (1993).

[17] Kyle, A. and Minchinton, A. Measurement of delivery and metabolism of tirapazamine to tumour tissue using multilayered cell culture model. Cancer Chemother Pharmacol **43**, 213-220 (1999).

[18] Hicks, K. et al. Multicellular resistance to tirapazamine is due to restricted extravascular transport: a pharmacokinetic/pharmacodynamic study in HT29 multicellular layer cultures. Cancer Research **63**, 5970-5977 (2003).

[19] Siim, B.G., van Zijl, P.L. and Brown, J.M. Tirapazamine-induced DNA damage measured using the comet assay correlates towards hypoxic tumour cells *in vitro*. British Journal of Cancer **73**, 952-960 (1996).

[20] Brown, J.M. The Hypoxic Cell: A Target for Selective Cancer Therapy – Eighteenth Bruce F. Cain Memorial Award Lecture. Cancer Research **59**, 5863-5870 (1999).

[21] Ngan, R.K. et al. Combination gemcitabine and cisplatin chemotherapy for metastatic or recurrent nasopharyngeal carcinoma: report of a phase II study. Annals of Oncology **13**, 1252-1258 (2002).

[22] Vanhoefer, U. et al. Schedule-dependent Antagonism of Paclitaxel and Cisplatin in Human Gastric and Ovarian Carcinoma Cell Lines In Vitro. European Journal of Cancer **31A**, 92-97 (1995).

[23] Zielinski, C. et al. Gemcitabine, Epirubicin and Paclitaxel Versus Fluorouracil, Epirubicin, and Cyclophosphamide As First-Line Chemotherapy in Metastatic Breast Cancer: A Central European Cooperative Oncology Group International, Multicenter, Prospective, Randomized Phase III Trial. Journal of Clinical Oncology **23**, 1401-1408 (2005).

[24] Sandstrom, M. et al. Population analysis of the pharmacokinetics and the haematological toxicity of the fluorouracil-epirubicin-cyclophosphamide regimen in breast cancer patients. Cancer Chemother Pharmacol **58**, 143-156 (2006).

[25] Bonneterre, J. et al. Phase II multicentre randomized study of docetaxel plus epirubicin vs 5-fluorouracil plus epirubicin and cyclophosphamide in metastatic breast cancer. British Journal of Cancer **91**, 1466-1471 (2004).

[26] Rougier, Ph. et al. Metastatic Carcinoid and Islet Cell Tumours of the Pancreas: a Phase II Trial of the Efficacy of Combination Chemotherapy with 5-Fluorouracil Doxorubicin and Cisplatin. Eur J Cancer **27**, 1380-1382 (1991).

[27] Fogli, S. et al. Gemcitabine, epirubicin and paclitaxel: Pharmacokinetic and pharmcodynamic interactions in advanced breast cancer. Ann Oncol **13**, 919-927 (2002).

[28] Seidman, AD. Monotherapy options in the management of metastatic breast cancer. Semin Oncol **30**, 6-10 (2003).

[29] Conte, PF. et al. Gemcitabine plus epirubicin plus Taxol (GET) in advanced breast cancer: A phase II study. Breast Cancer Res Treat **68**, 171-179 (2001).

[30] Rafi, I. *An introduction to the use of anticancer drugs* (Elsevier, New York, 2006).

[31] Jordan, P. and Carmo-Fonseca, M. Molecular mechanisms involved in cisplatin cytotoxicity. Cellular and Molecular Life Sciences **57**, 1229-1235 (2000).

[32] Lu, Q.-B., Kalantari, S. and Wang, C.-R. Electron Transfer Reaction Mechanism of Cisplatin with DNA at the Molecular Level. Molecular Pharmaceutics **4**, 624-628 (2007).

[33] Lu, Q.-B. Molecular Reaction Mechanisms of Combination Treatments of Low-Dose Cisplatin with Radiotherapy and Photodynamic Therapy. J. Med. Chem. **50**, 2601-2604 (2007).

[34] Gelasco, A. and Lippard, S.J. NMR solution structure of a DNA dodecamer duplex containing a cis-diammineplatinum(II) d(GpG) intrastrand cross-link, the major adduct of the anticancer drug cisplatin. Biochemistry **37**, 9230-9239 (1998).

[35] Takahara, P. et al. Crystal structure of double-stranded DNA containing the major adduct of the anticancer drug cisplatin. Nature **377**, 649-652 (1995).

[36] Miller, S.E. and House, D.A. The hydrolysis products of cis-dichlorodiammineplatinum(II) 3. Hydrolysis kinetics at physiological pH. Inorg. Chim. Acta. **173**, 53-60 (1990).

[37] Berners-Price, S.J. et al. Hydrolysis products of cisplatin: pK_a determination via [^{1}H, ^{15}N] NMR spectroscopy. J. Chem. Soc., Chem. Commun., 789-791 (1992).

[38] Christophorou, L.G., McCorkle, D.L. and Christodoulides, A.A. *Electron-Molecule Interactions and Their Applications*. (Academic Press, Orlando, 1984).

[39] Dixon-Warren, S.J., Jensen, E.T. and Polanyi, J.C. Direct evidence for charge-transfer photodissociation at a metal-surface-CCl_4/Ag-(111). Physical Review Letters **67**, 2395-2398 (1991).

[40] Illenberger, E. Electron-attachment reactions in molecular clusters. Chem. Rev. **92**, 1589-1609 (1992).

[41] Illenberger, E. et al. Dissociative electron-attachment to condensed and adsorbed halomethanes. J. Chem. Phys. **101**, 4248-4259 (1994).

[42] Lu, Q.-B. and Madey, T.E. Negative-ion enhancements in electron-stimulated desorption of CF_2Cl_2 coadsorbed with nonpolar and polar gases on Ru(0001). Phys. Rev. Lett. **82**, 4122-4125 (1999).; Lu, Q.-B. and Madey, T.E. Giant enhancement of electron-induced dissociation of chlorofluorocarbons coadsorbed with water or ammonia ices: Implications for the atmospheric ozone depletion. J. Chem. Phys. **111**, 2861-2864 (1999).

[43] Lu, Q.-B. and Sanche, L. Enhanced Dissociative Electron Attachment to CF_2Cl_2 by Transfer of Electrons Localized in Preexisting Traps of Water and Ammonia Ice. Phys. Rev. B. **63**, 153403-153406 (2001).

[44] Jacobs, C. et al. A phase III randomized study comparing cisplatin and fluorouracil as single agents and in combination for advanced squamous cell carcinoma of the head and neck [Abstract]. Journal of Clinical Oncology **10**, 257-263 (1992).

[45] Kim, Y. et al. Paclitaxel, 5-Fluorouracil, and Cisplatin Combination Chemotherapy for the Treatment of Advanced Gastric Carcinoma. Cancer **85**, 295-301 (1999).

[46] Chaudhry, V. et al. Peripheral Neuropathy from Taxol and Cisplatin Combination Chemotherapy: Clinical and Electrophysiological Studies. Annals of Neurology **35**, 304-311 (1994).

[47] Kano, Y. et al. In vitro schedule-dependent interaction between paclitaxel and cisplatin in human carcinoma cell lines. Cancer Chemother Pharmacol **37**, 525-530 (1996).

[48] Jekunen, A.P. et al. Synergistic interaction between cisplatin and taxol in human ovarian carcinoma cells in vitro. British Journal of Cancer **69**, 299-306 (1994).

[49] Thigpen, J.T. et al. Phase II trial of paclitaxel in patients with progressive ovarian carcinoma after platinum-based chemotherapy: a Gynecologic Oncology Group study. Journal of Clinical Oncology **12**, 1748-1753 (1994).

[50] McGuire, W. et al. Cyclophosphamide and cisplatin compared with paclitaxel and cisplatin in patients with stage III and stage IV ovarian cancer. The New England Journal of Medicine **334**, 1-6 (1996).

[51] Ilson, D.H. et al. A phase II trial of paclitaxel and cisplatin in patients with advanced carcinoma of the esophagus. Cancer Journal **6**, 316-323 (2000).

[52] Crino, L. et al. Cisplatin-gemcitabine combination in advanced non-small-cell lung cancer: a phase II study. Journal of Clinical Oncology **15**, 297-303 (1997).

[53] Bergmen, A.M. et al. Synergistic Interaction between Cisplatin and Gemcitabine *in vitro*. Clinical Cancer Research **2**, 521-530 (1996).

[54] Crul, M. et al. DNA repair mechanisms involved in gemcitabine cytotoxicity and in the interaction between gemcitabine and cisplatin. Biochemical Pharmacology **65**, 275-282 (2003).

[55] Peters, G.J. et al. Interaction between cisplatin and gemcitabine in vitro and in vivo. Semin Oncol **22**, 72-79 (1995).

[56] Moufarij, M., Phillips, D. and Cullinane, C. Gemcitabine Potentiates Cisplatin Cytotoxicity and Inhibits Repair of Cisplatin-DNA Damage in Ovarian Cancer Cell Lines. Molecular Pharmcology **63**, 862-869 (2003).

[57] Chia, W.K. et al. Phase II trial of gemcitabine in combination with cisplatin in inoperable or advanced hepatocellular carcinoma. Ann Acad Med Singapore **37**, 554-448 (2008).

[58] Markham, C., Stocken, D. and Hassan, A. A phase II irinotecan-cisplatin combination in advanced pancreatic cancer. British Journal of Cancer **89**, 1860-1864 (2003).

[59] Jurtshuk, P. Jr., McQuitty, D.N. and Riley, W.H. IV, Current Microbiology **2**, 349-354 (1979).

[60] Makin, G. and Hickman, J. Apoptosis and cancer chemotherapy. Cell Tissue Res **301**, 143-152 (2000).

[61] Vermeulen, K., Van Bockstaele, D.R. and Berneman, Z. The cell cycle: a review of regulation, deregulation and therapeutic targets in cancer. Cell Proliferation **36**, 131-149 (2003).

[62] King, K.L. and Cidlowski, J.A. Cell Cycle Regulation and Apoptosis. Annu. Rev. Physiol. **60**, 601-617 (1998).

[63] Shapiro, G. and Harper, J.W. Anticancer drug targets: cell cycle and checkpoint control. Journal of Clinical Investigation **104**, 1645-1653 (1999).

[64] Agami, R. and Bernards, R. Distinct initiation and maintenance mechanisms cooperate to induce g1 cell cycle arrest in response to DNA damage. Cell **102**, 55-77 (2000).

[65] Pozarowski, P. et al. Interactions of Fluorochrome-Labeled Caspase Inhibitors With Apoptotic Cells: A Caution in Data Interpretation. Cytometry Part A **55A**, 50-60 (2003).

[66] Horky, M. et al. Segregation of nucleolar components coincides with caspase-3 activation in cisplatin-treated HeLa cells. Journal of Cell Science **114**, 663-670 (2000).

[67] Collins, J. et al. Major DNA Fragmentation Is a Late Event in Apoptosis. The Journal of Histochemistry & Cytochemistry **45**, 923-934 (1997).

[68] Mosmann, T. Rapid Colorimetric Assay for Cellular Growth and Survival: Application to Proliferation and Cytotoxicity Assays. Journal of Immunological Methods **65**, 55-63 (1983).

[69] Franken, N. et al. Clonogenic assay of cells *in vitro*. Nature Protocols **1**, 2315-2319 (2006).

[70] Kamesaki, H. Mechanisms involved in chemotherapy-induced apoptosis and their implications in cancer chemotherapy. International Journal of Hematology **68**, 29-43 (1998).

[71] Minagawa, Y. et al. Cisplatin-resistant HeLa Cells Are Resistant to Apoptosis via p53-dependent and –independent Pathways. Jpn. J. Cancer Res. **90**, 1373-1379 (1999).

[72] Chu, G. Cellular responses to cisplatin. J. Biol. Chem. **269**, 787-790 (1994).

[73] Allday, M.J. et al. DNA damage in human B cells can induce apoptosis, proceeding from G1/S when p53 is transactivation competent and G2/M when it is transactivation defective. EMBO J. **14**, 4994-5005 (1995).

[74] Van Dilla, M., et al. *Flow Cytometry: Instrumentation and Data Analysis* (Academic Press, London, 1985).

[75] Yamada, M. and Puck, T. Action of radiation on mammalian cells, IV. Reversible mitotic lag in the S3 Hela cell produced by low doses of X-rays. Proceedings of the National Academy of Sciences **47**, 1181-1191 (1961).

[76] Chen, C.-Y. et al. (-)-Anonaine induces apoptotis through Bax- and caspase-dependent pathways in human cervical cancer (HeLa) cells. Food and Chemical Toxicology **46**, 2694-2702 (2008).

[77] Nihal, M. et al. Anti-proliferative and proapoptotic effects of (-)-epigallocatechin-3-gallate on human melanoma: Possible implications for the chemoprevention of melanoma. Int. J. Cancer **114**, 513-521 (2005).

[78] Hanahan, D. and Weinberg, R. The Hallmarks of Cancer. Cell **100**, 57-70 (2000).

[79] Schwartz, G. *Combination Cancer Therapy: Modulators and Potentiators* (Humana Press, New Jersey, 2005).